buildings

MDPI

*Article*

# Size Dependent Buckling Analysis of a FG-CNTRC Microplate of Variable Thickness under Non-Uniform Biaxial Compression

**Pouyan Roodgar Saffari [1,*], William Sher [2] and Chanachai Thongchom [1,*]**

[1] Department of Civil Engineering, Thammasat School of Engineering, Faculty of Engineering, Thammasat University, Pathumthani 12120, Thailand
[2] School of Civil, Mining & Environmental Engineering, Faculty of Engineering and Information Sciences, University of Wollongong, Newcastle, NSW 2522, Australia
* Correspondence: rpouyan@engr.tu.ac.th (P.R.S.); tchanach@engr.tu.ac.th (C.T.)

**Abstract:** This paper combines third-order shear deformation theory (TSDT) and modified couple stress theory (MCST) with the principle of total potential energy to analyze the size-dependent buckling behavior of a functionally graded carbon nanotube-reinforced composite (FG-CNTRC) rectangular microplate of variable thickness subject to non-uniform biaxial compression when resting on an elastic medium. To determine the thickness qualities of the material, the extended rule of mixture was applied. In the context of microplate buckling in the presence of small length scale effects, the three kinds of Carbon Nanotube (CNT) distribution—(a) UD, (b) FG-O, and (c) FG-X—were used and compared. The equations governing various combinations of simply supported or clamped boundary conditions have been solved using the differential quadrature method (DQM). The correctness and precision of the solutions have been compared to another study. A numerical study was conducted to examine the dependence of buckling load on several parameters, including percentage change of thickness, length scale parameter, nonuniform edge loads, boundary conditions, volume percentage of the CNTs, CNT distribution, and elastic medium parameter. The results of their effects are presented in this paper.

**Keywords:** modified couple stress theory; FG-CNTRC microplate; biaxial buckling; nonuniform edge compression; nonuniform cross-section



**Citation:** Roodgar Saffari, P.; Sher, W.; Thongchom, C. Size Dependent Buckling Analysis of a FG-CNTRC Microplate of Variable Thickness under Non-Uniform Biaxial Compression. *Buildings* **2022**, *12*, 2238. https://doi.org/10.3390/buildings12122238

Academic Editor: André Rafael Dias Martins

Received: 8 November 2022
Accepted: 13 December 2022
Published: 15 December 2022



## 1. Introduction

Both uniform and non-uniform plates are used in a wide variety of engineering contexts. Designers can accomplish this by using structures of varying thicknesses. Such plates are optimal when minimizing mass is crucial, as is the case with space-based construction. Compressive pressures cause plates to buckle, and knowing how devices behave under stress is crucial to making good design decisions [1]. Most buckling research investigates evenly distributed uniaxial and biaxial in-plane loads and is based on several plate theories [2–6]. Hamedani and Ranji [7] investigated the buckling analysis of stiffened plates exposed to varied biaxial edge compressions under different boundary conditions using super and conventional elements. Ruocco and Reddy [8] proposed an innovative discrete differential geometry-based computational method for buckling and vibration studies of non-uniformly thick rectangular plates. The bending, buckling, stress, and failure strength in inter-ply hybrid laminated composite have been investigated [9] using an isogeometric analysis based on non-uniform rational B-spline (NURBS) basis functions.

Structures of micron and submicron scales are widely used in many modern contexts, particularly in microelectromechanical systems (MEMS). Due to their small size, low power requirements, and reliable batch manufacture, these systems offer a wide range of possible engineering applications [10,11]. Lacking an intrinsic material length scale characteristic, classical continuum models are unable to account for size effects. Various size-dependent

theories have been established in recent years, including the couple stress theory (CST) [12], the nonlocal elasticity theory [13,14], the strain gradient theory (SGT) [15,16], the modified strain gradient theory (MSGT) [17], the nonlocal strain gradient theory (NSGT) [18–23], and the modified couple stress theory (MCST) [24]. Among these size-dependent theories, MCST requires only a material length scale parameter, making it easy to implement. By eliminating the dilatation gradient tensor and the deviatoric stretch gradient tensor from SGT, as shown by MSCT, the size effect is shown to be a function of an internal length scale parameter. A variety of size-dependent beam and plate models, including the Timoshenko beam model [25,26], Kirchhoff plate model [27,28], Mindlin plate model [29–31], size-dependent Euler–Bernoulli beam model [32,33], and higher order shear deformable plate model [34,35] have recently been developed using MCST. Based on MCST in conjunction with TSDT, Thanh et al. [36] developed a numerical model to analyze the thermal bending and thermal buckling of composite laminate microplates while taking into account the effects of scale. Lou et al. [37] applied MSCT and first shear deformation theory (FSDT) to evaluate the vibrational dynamics of a buckled FG microplate supported by a nonlinear elastic medium. Zhang et al. [38] examined the mechanical buckling of a microplate consisting of two piezoelectric face sheets and one honeycomb structure considering MCST and sinusoidal shear deformation theory (SSDT). The effective mechanical characteristics of the honeycomb core were calculated using the Minghui and Jiuren relationships. Afshari and Adab [39] performed size-dependent mechanical buckling and free vibration calculations on simply supported microplates reinforced by FG graphene nanoplatelets using MCST SSDT. It was assumed that the composite microplate was made up of epoxy reinforced by GNPs, which were then arranged in a variety of symmetric and non-symmetric patterns along the thickness axis. By combining the Halpin–Tsai model and the rule of mixtures, they were able to make an educated assessment of the effective material qualities of the composite microplate.

Carbon nanotubes (CNTs) are a class of unique materials that exhibit remarkable electro-thermo-mechanical properties, and they have been receiving more and more attention in recent years [40–43]. CNTs are an attractive option for composite matrix reinforcement. The CNTs can be employed in a variety of technical applications when combined with a polymer composite material to create carbon nanotube reinforced composites (CNTRCs). Because of the uniform or random distribution of reinforcements within the system, the mechanical, physical, and thermal properties of conventional composites do not change spatially at the visible level. Functionally graded materials (FGMs) [44–46] have been created to improve this property. They have two or more elements with spatially variable characteristics and a non-uniform reinforcement distribution. Vaishali et al. [47] aligned between first-order shear deformation theory and higher-order zigzag theory using data and machine learning. This enabled uncertainty to be measured with a high degree of accuracy for laminated composite and sandwich plates. The reanalysis algorithm is a quick and precise solution that Li [48] applied to the vibration problem and incorporated to increase the effectiveness of metaheuristic optimization of composite laminates instead of a surrogate model. Savran and Aydin [49] used stochastic optimization on a laminated composite made of graphite, flax, and epoxy to obtain the highest fundamental frequency and lowest cost. Engineers can use this method to create materials better than homogenous ones. Shen [50] demonstrated that CNTRCs with nonuniform dispersion of CNTs through the media can be created by a powder metallurgy production process. Functionally graded carbon nanotube-reinforced composite is the name given to this type of reinforced composite media (FG-CNTRC). In recent years, more research has been conducted on these engineered materials in a variety of combinations to better understand their behavior in static and dynamic settings. The elastic instability and free vibration of FG-CNTRC annular sector plates on an elastic medium were presented by Zhang et al. [51] using FSDT and a generalized differential quadrature (GDQ) approach. Thai et al. [52] presented a size-dependent computational technique for static bending and free vibration studies of FG-CNTRC microplates based on MSGT and higher-order shear deformation theory.

Cheshmeh et al. [53] investigated the buckling and vibration analysis of an FG-CNTRC rectangular plate under different temperature distributions and boundary conditions using the 12-uncertainty higher order shear deformation theory (HSDT). According to NSGT and isogeometric analysis (IGA), Phung-Van and Thai [54] predicted the natural frequencies of FG-CNTRC nanoplates employing HSDT.

Despite the extensive research on the uniaxial and biaxial buckling characteristics of composite microplates, the literature presented here shows that the buckling behavior of an FG-CNTRC microplate of varying thickness subjected to non-uniform biaxial compression resting on an elastic medium based on the TSDT in conjunction with MCST has not been studied theoretically or numerically. The main goal of the current research is to fill this gap by providing a novel combination of many existing methodologies. The three different types of CNT distribution—(a) UD, (b) FG-O, and (c) FG-X—are used and compared in the context of microplate buckling in the presence of small length scale effects. Total potential energy is used to obtain the governing equations, which are then solved by DQM for various combinations of simply supported or clamped boundary conditions.

## 2. Problem Description and Modeling

As can be seen in Figure 1, an FG-CNTRC microplate ($a \times b$) is subjected to biaxial non-uniform edge compression as its thickness varies in the y-direction (y-axis) while resting on an elastic medium with the stiffness coefficient $k_w$. Furthermore, $h_1$ indicates the thickness of the FG-CNTRC microplate's left end, while $h_0$ represents the thickness of the right side of the FG-CNTRC microplate. In this illustration, UD represents the uniform distribution. FG-O and FG-X are two distinct FG distributions in the plate thickness direction.

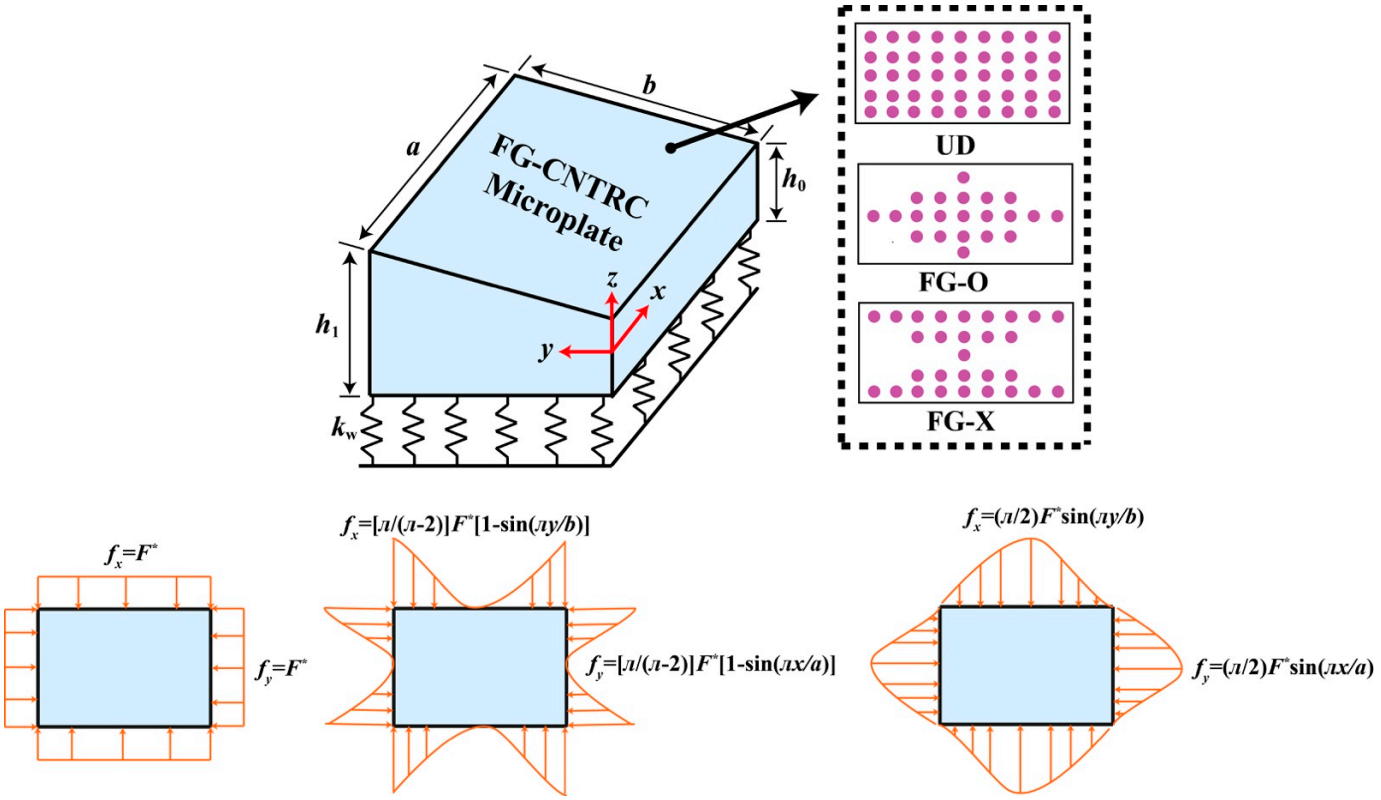


**Figure 1.** Configuration of an FG-CNTRC microplate resting on an elastic medium subjected to biaxial uniform and non-uniform edge compression loads.

### 2.1. MCST

Yang et al. [24] were the first to present MCST. Here, the strain energy density is analyzed as a function of the stress tensor, the curvature tensor, and the couple stress tensor.

In an isotropic linear elastic body that occupies region $\Lambda$, the strain energy $\Pi_s$ may then be expressed as

$$\Pi_s = \frac{1}{2}\int_{\Lambda}(\sigma : \varepsilon + m : \chi)\Lambda \tag{1}$$

Here, $\varepsilon$ signifies the strain tensor, $\varepsilon$ represents the Cauchy stress tensor, $\chi$ represents the symmetric curvature tensor, and m represents the deviatoric component of the couple stress tensor. Specifically, these tensors are characterized by [24]

$$\begin{aligned} &\varepsilon = \tfrac{1}{2}\left[\nabla \mathrm{u} + (\nabla \mathrm{u})^{\mathrm{T}}\right],\ \chi = \tfrac{1}{2}\left[\nabla \varphi + (\nabla \varphi)^{\mathrm{T}}\right], \\ &\sigma = \lambda \mathrm{tr}(\varepsilon)\mathrm{I} + 2\mu\varepsilon,\ m = 2l^2\mu\ \chi, \end{aligned} \tag{2}$$

where $l$ is a material length scale parameter that is considered to be a material feature describing the influence of the coupling stress, u is the displacement vector, $\lambda$ and $\mu$ are Lame's constants, and $\varphi = \frac{1}{2}\mathrm{curl}(u)$ is the rotation vector. In this model, in addition to the standard Lame's constants, only one length scale parameter $l$ is required. It should be noted that the additional parameter $l$ is technically the square of the modulus of curvature/modulus of the shear ratio and physically a property measuring the influence of couple stress.

### *2.2. Structural Model*

Both shear deformation and rotating inertia in the transverse direction are taken into account by TSDT. Total lateral displacement (U,V,W) in Cartesian coordinates for microplate can be shown as [55,56]

$$\begin{aligned} U(x,y,z) &= u(x,y) + z\theta_x(x,y) - C_1 z^3\left(\theta_x(x,y) + \tfrac{\partial w(x,y)}{\partial x}\right), \\ V(x,y,z) &= v(x,y) + z\theta_y(x,y) - C_1 z^3\left(\theta_y(x,y) + \tfrac{\partial w(x,y)}{\partial y}\right), \\ W(x,y,z) &= w(x,y) \end{aligned} \tag{3}$$

in which $C_1 = \frac{4}{3h^2(y),}$. In addition, $w$ is the transverse displacement component; $\theta_x$ and $\theta_y$ represent rotations of the middle plane around the x- and y-axes, respectively; and u and v are the membrane displacements along the x- and y-axes, respectively. However, using the linear strain-displacement connection, the specific components of the normal strains $(\varepsilon_{xx},\ \varepsilon_{yy})$ and shear strains $(\gamma_{xz},\ \gamma_{yz}, \gamma_{xy})$ are stated as follows:

$$\begin{aligned} \varepsilon_{xx} &= \tfrac{\partial u}{\partial x} + z\tfrac{\partial \theta_x}{\partial x} - c_1 z^3\left(\tfrac{\partial \theta_x}{\partial x} + \tfrac{\partial^2 w}{\partial x^2}\right), \\ \varepsilon_{yy} &= \tfrac{\partial v}{\partial y} + z\tfrac{\partial \theta_y}{\partial y} - c_1 z^3\left(\tfrac{\partial \theta_y}{\partial y} + \tfrac{\partial^2 w}{\partial y^2}\right), \\ \gamma_{xy} &= \tfrac{\partial u}{\partial y} + \tfrac{\partial v}{\partial x} + z\left(\tfrac{\partial \theta_x}{\partial y} + \tfrac{\partial \theta_y}{\partial x}\right) - c_1 z^3\left(\tfrac{\partial \theta_x}{\partial y} + \tfrac{\partial \theta_y}{\partial x} + 2\tfrac{\partial^2 w}{\partial x \partial y}\right), \\ \gamma_{xz} &= \left(1 - 3c_1 z^2\right)\left(\theta_x + \tfrac{\partial w}{\partial x}\right), \\ \gamma_{yz} &= \left(1 - 3c_1 z^2\right)\left(\theta_y + \tfrac{\partial w}{\partial y}\right) \end{aligned} \tag{4}$$

The rotation vector is calculated by substituting the results of Equations (1) and (2) into Equation (2) as

$$\begin{aligned}
\varphi_x &= \frac{1}{2}\left(\frac{\partial W}{\partial y} - \frac{\partial V}{\partial z}\right) = \frac{1}{2}\left(\left[\frac{\partial w}{\partial y} - \theta_y\right] + 3C_1 z^2\left[\theta_y + \frac{\partial w}{\partial y}\right]\right),\\
\varphi_y &= \frac{1}{2}\left(\frac{\partial U}{\partial z} - \frac{\partial W}{\partial x}\right) = -\frac{1}{2}\left(\left[\frac{\partial w}{\partial x} - \theta_x\right] + 3C_1 z^2\left[\theta_x + \frac{\partial w}{\partial x}\right]\right),\\
\varphi_z &= \frac{1}{2}\left(\frac{\partial V}{\partial x} - \frac{\partial U}{\partial y}\right) = \frac{1}{2}\left(\left[\frac{\partial v}{\partial x} - \frac{\partial u}{\partial y}\right] + \left(z - C_1 z^3\right)\left[\frac{\partial \theta_y}{\partial x} - \frac{\partial \theta_x}{\partial y}\right]\right).\\
\chi_x &= \frac{1}{2}\left(\frac{\partial^2 w}{\partial x \partial y} - \frac{\partial \theta_y}{\partial x}\right) + \frac{3C_1 z^2}{2}\left[\frac{\partial \theta_y}{\partial x} + \frac{\partial^2 w}{\partial x \partial y}\right],\\
\chi_y &= -\frac{1}{2}\left(\frac{\partial^2 w}{\partial x \partial y} - \frac{\partial \theta_x}{\partial y}\right) - \frac{3C_1 z^2}{2}\left(\frac{\partial \theta_x}{\partial y} + \frac{\partial^2 w}{\partial x \partial y}\right),\\
\chi_z &= \frac{1-3C_1 z^2}{2}\left(\frac{\partial \theta_y}{\partial x} - \frac{\partial \theta_x}{\partial y}\right),\\
\chi_{xy} &= \frac{1+3C_1 z^2}{4}\left(\frac{\partial^2 w}{\partial y^2} - \frac{\partial^2 w}{\partial x^2}\right) + \frac{1-3C_1 z^2}{4}\left(\frac{\partial \theta_x}{\partial x} - \frac{\partial \theta_y}{\partial y}\right),\\
\chi_{xz} &= \frac{1}{4}\left(\frac{\partial^2 v}{\partial x^2} - \frac{\partial^2 u}{\partial x \partial y}\right) + \frac{z - C_1 z^3}{4}\left(\frac{\partial^2 \theta_y}{\partial x^2} - \frac{\partial^2 \theta_x}{\partial x \partial y}\right) + \frac{3C_1 z}{2}\left(\theta_y + \frac{\partial w}{\partial y}\right),\\
\chi_{yz} &= \frac{1}{4}\left(-\frac{\partial^2 u}{\partial y^2} + \frac{\partial^2 v}{\partial x \partial y}\right) + \frac{z - C_1 z^3}{4}\left(\frac{\partial^2 \theta_y}{\partial x \partial y} - \frac{\partial^2 \theta_x}{\partial y^2}\right) - \frac{3C_1 z}{2}\left(\theta_x + \frac{\partial w}{\partial x}\right).
\end{aligned} \tag{5}$$

Based on Equation (2), the strain–stress relationship for the FG-CNTRC microplate in the plain stress state can be written as:

$$\begin{bmatrix} \sigma_{xx} \\ \sigma_{yy} \\ \sigma_{xy} \\ \sigma_{yz} \\ \sigma_{xz} \end{bmatrix} = \begin{Bmatrix} Q_{11} & Q_{12} & 0 & 0 & 0 \\ Q_{21} & Q_{22} & 0 & 0 & 0 \\ 0 & 0 & Q_{66} & 0 & 0 \\ 0 & 0 & 0 & Q_{44} & 0 \\ 0 & 0 & 0 & 0 & Q_{55} \end{Bmatrix} \begin{bmatrix} \varepsilon_{xx} \\ \varepsilon_{yy} \\ \gamma_{xy} \\ \gamma_{yz} \\ \gamma_{xz} \end{bmatrix}, \tag{6}$$
$$Q_{11} = \frac{E_{11}}{1-\vartheta_{12}\vartheta_{21}},\ Q_{22} = \frac{E_{22}}{1-\vartheta_{12}\vartheta_{21}},\ Q_{12} = \frac{\vartheta_{12}E_{22}}{1-\vartheta_{12}\vartheta_{21}},\ Q_{66} = G_{12}, Q_{44} = G_{23},\ Q_{55} = G_{13}$$

Here, $E_{11}$ and $E_{22}$ express the effective Young's modulus of the FG-CNTRC microplate, $\vartheta_{12}$ and $\vartheta_{21}$ stand for Poisson's ratio, while $G_{12}$, $G_{23}$, and $G_{13}$ denote the shear modulus. Applying the rule of mixture, we can characterize the material properties of the FG-CNTRC plate as [57]

$$\begin{aligned}
E_{11} &= \zeta_1 V_{CNT} E_{11}^{CNT} + V_m E_m,\\
\frac{\zeta_2}{E_{22}} &= \frac{V_{CNT}}{E_{22}^{CNT}} + \frac{V_m}{E_m},\\
\frac{\zeta_3}{G_{12}} &= \frac{V_{CNT}}{G_{12}^{CNT}} + \frac{V_m}{G_m},
\end{aligned} \tag{7}$$

where $(E_m, G_m)$ represent the isotropic matrix moduli, and $\left(E_{11}^{CNT}, E_{22}^{CNT}, G_{12}^{CNT}\right)$ represent the material characteristics of CNTs. Furthermore, the CNT efficiency characteristics are denoted by $\zeta_1$, $\zeta_2$, and $\zeta_3$, and

$$\begin{aligned}
V_m + V_{CNT} &= 1,\\
\vartheta_{12} &= V_{CNT}^{*}\vartheta_{12}^{CNT} + V_m\vartheta_m,
\end{aligned} \tag{8}$$

where $V_{CNT}^{*}$ and $V_{CNT}$ denote the volume percentages of each FG-CNTRC layer, which can be expressed for three types of CNT distribution as UD, FG-O, and FG-X [57]:

$$V_{CNT} = \begin{cases} V_{CNT}^{*} & (\mathrm{UD}) \\ 2\left(1 - \frac{2|z|}{h_c}\right)V_{CNT}^{*}, & (\mathrm{FG-O}) \\ 4\frac{|z|}{h_c}V_{CNT}^{*}, & (\mathrm{FG-X}) \end{cases} \tag{9}$$

The total potential energy concept is applied to derive the FG-CNTRC microplate equilibrium equations as

$$\delta\Big(\Pi_s + \Pi_f\Big) = 0 \tag{10}$$

where $\delta$ refers to a variation with regard to both $x$ and $y$. The total energy of deformations is denoted by $\Pi_s$, and the virtual work done by external forces is denoted by $\Pi_f$. The variation of the total strain energy based on Equation (1) can be expressed as

$$\begin{aligned}
\delta\Pi_s = \int_A \; & \int_{-\frac{h(y)}{2}}^{\frac{h(y)}{2}} (\sigma_{xx}\delta\varepsilon_{xx} + \sigma_{yy}\delta\varepsilon_{yy} + \sigma_{xy}\delta\gamma_{xy} + \sigma_{yz}\delta\gamma_{yz} + \sigma_{xz}\delta\gamma_{xz} + m_x\delta\chi_x + m_y\delta\chi_y \\
& + m_z\delta\chi_z + 2m_{xy}\delta\chi_{xy} + 2m_{xz}\delta\chi_{xz} + 2m_{yz}\delta\chi_{yz})dzdA \\
& = \int_S \Big\{ N_x\delta\frac{\partial u}{\partial x} + (M_x - C_1P_x)\delta\frac{\partial\theta_x}{\partial x} - C_1P_x\delta\frac{\partial^2 w}{\partial x^2} + N_y\delta\frac{\partial v}{\partial y} \\
& + \big(M_y - C_1P_y\big)\delta\frac{\partial\theta_y}{\partial y} - C_1P_y\delta\frac{\partial^2 w}{\partial y^2} + N_{xy}\Big(\frac{\delta\partial u}{\partial y} + \frac{\delta\partial v}{\partial x}\Big) \\
& + \big(M_{xy} - C_1P_{xy}\big)\Big(\frac{\delta\partial\theta_x}{\partial y} + \frac{\delta\partial\theta_y}{\partial x}\Big) - 2C_1P_{xy}\frac{\delta\partial^2 w}{\partial x\partial y} \\
& + (Q_x - 3C_1R_x)\Big(\delta\theta_x + \frac{\delta\partial w}{\partial x}\Big) + \big(Q_y - 3C_1R_y\big)\Big(\delta\theta_y + \frac{\delta\partial w}{\partial y}\Big) \\
& + \frac{X_x}{2}\Big(\frac{\delta\partial^2 w}{\partial x\partial y} - \frac{\delta\partial\theta_y}{\partial x}\Big) + \frac{3C_1Z_x}{2}\Big(\frac{\delta\partial^2 w}{\partial x\partial y} + \frac{\delta\partial\theta_y}{\partial x}\Big) - \frac{X_y}{2}\Big(\frac{\delta\partial^2 w}{\partial x\partial y} - \frac{\delta\partial\theta_x}{\partial y}\Big) \\
& - \frac{3C_1Z_y}{2}\Big(\frac{\delta\partial^2 w}{\partial x\partial y} + \frac{\delta\partial\theta_x}{\partial y}\Big) + \frac{X_z - 3C_1Z_{xy}}{2}\Big(\frac{\delta\partial\theta_y}{\partial x} - \frac{\delta\partial\theta_x}{\partial y}\Big) \\
& + \frac{X_{xy} + 3C_1Z_{xy}}{2}\Big(\frac{\delta\partial^2 w}{\partial y^2} - \frac{\delta\partial^2 w}{\partial x^2}\Big) + \frac{X_{xy} - 3C_1Z_{xy}}{2}\Big(\frac{\delta\partial\theta_x}{\partial x} - \frac{\delta\partial\theta_y}{\partial y}\Big) \\
& + \frac{X_{xz}}{2}\Big(\frac{\delta\partial^2 v}{\partial x^2} - \frac{\delta\partial^2 u}{\partial x\partial y}\Big) + \frac{Y_{xz} - C_1W_{xz}}{2}\Big(\frac{\delta\partial^2\theta_y}{\partial x^2} - \frac{\delta\partial^2\theta_x}{\partial x\partial y}\Big) \\
& + 3C_1Y_{xz}\Big(\delta\theta_y + \frac{\delta\partial w}{\partial y}\Big) + \frac{X_{yz}}{2}\Big(\frac{\delta\partial^2 v}{\partial x\partial y} - \frac{\delta\partial^2 u}{\partial y^2}\Big) \\
& + \frac{Y_{yz} - C_1W_{yz}}{2}\Big(\frac{\delta\partial^2\theta_y}{\partial x\partial y} - \frac{\delta\partial^2\theta_x}{\partial y^2}\Big) - 3C_1Y_{yz}\Big(\delta\theta_x + \frac{\delta\partial w}{\partial x}\Big)\Big\}dA
\end{aligned} \tag{11}$$

where $A$ is the of cross-sectional area, and

$$\begin{aligned}
\{N_i, M_i, P_i\} &= \int_{-\frac{h}{2}}^{\frac{h}{2}} \{1, z, z^3\}\sigma_i dz, \;\; i = x, y, xy, \\
\{Q_i, R_i\} &= \int_{-\frac{h}{2}}^{\frac{h}{2}} \{1, z^2\}\sigma_{iz} dz, \;\; i = x, y, \\
\{X_i, Y_i, Z_i, W_i\} &= \int_{-\frac{h}{2}}^{\frac{h}{2}} \{1, z, z^2, z^3\} m_i dz,
\end{aligned} \tag{12}$$

The potential energy variation caused by non-uniform forces and the elastic medium can be expressed as

$$\delta\Pi_f = \int \left( -f_x\left(\frac{\partial^2 w}{\partial x^2}\right) - f_y\left(\frac{\partial^2 w}{\partial y^2}\right) - 2f_{xy}\left(\frac{\partial^2 w}{\partial x\partial y}\right) + K_w w\right)\delta w dA \tag{13}$$

in which the compressive forces in the x and y directions are denoted by $f_x$ and $f_y$, respectively, while the shear force is denoted by $f_{xy}$. The final form of the governing equations is determined by inserting Equations (11) and (13) into Equation (10) and performing various manipulations while keeping the coefficients $\delta u$, $\delta v$, $\delta w$, $\delta\theta_x$, and $\delta\theta_y$ equal to zero.

$$
\begin{aligned}
&\delta u: \ \frac{\partial N_x}{\partial x}+\frac{\partial N_{xy}}{\partial y}+\frac{1}{2}\left(\frac{\partial^2 X_{xz}}{\partial x\partial y}+\frac{\partial^2 X_{yz}}{\partial y^2}\right)=0,\\
&\delta v: \ \frac{\partial N_y}{\partial y}+\frac{\partial N_{xy}}{\partial x}-\frac{1}{2}\left(\frac{\partial^2 X_{xz}}{\partial x^2}+\frac{\partial^2 X_{yz}}{\partial x\partial y}\right)=0,\\
&\delta w_0: \ \frac{\partial Q_x}{\partial x}-3C_1\frac{\partial R_x}{\partial x}+\frac{\partial Q_y}{\partial y}-3C_1\frac{\partial R_y}{\partial y}+C_1\left(\frac{\partial^2 P_x}{\partial x^2}+2\frac{\partial^2 P_{xy}}{\partial x\partial y}+\frac{\partial^2 P_y}{\partial y^2}\right)+3C_1\left(\frac{\partial Y_{xz}}{\partial y}-\frac{\partial Y_{yz}}{\partial x}\right)+\frac{1}{2}\left(\frac{\partial^2 X_{xy}}{\partial x^2}+\right.\\
&\left.3C_1\frac{\partial^2 Z_{xy}}{\partial x^2}-\frac{\partial^2 X_{xy}}{\partial y^2}-3C_1\frac{\partial^2 Z_{xy}}{\partial y^2}+\frac{\partial^2 X_y}{\partial x\partial y}+3C_1\frac{\partial^2 Z_y}{\partial x\partial y}-\frac{\partial^2 X_x}{\partial x\partial y}-3C_1\frac{\partial^2 Z_x}{\partial x\partial y}\right)-f_x\left(\frac{\partial^2 w}{\partial x^2}\right)-f_y\left(\frac{\partial^2 w}{\partial y^2}\right)-\\
&2f_{xy}\left(\frac{\partial^2 w}{\partial x\partial y}\right)+K_w w=0,\\
&\delta\theta_x: \ \frac{\partial M_x}{\partial x}-C_1\frac{\partial P_x}{\partial x}+\frac{\partial M_{xy}}{\partial y}-C_1\frac{\partial P_{xy}}{\partial y}-(Q_x-3C_1R_x)+\frac{1}{2}\left(\frac{\partial X_{xy}}{\partial x}-3C_1\frac{\partial Z_{xy}}{\partial x}+\frac{\partial X_y}{\partial y}-3C_1\frac{\partial Z_y}{\partial y}-\frac{\partial X_z}{\partial y}+\right.\\
&\left.3C_1\frac{\partial Z_z}{\partial y}+\frac{\partial^2 Y_{xz}}{\partial x\partial y}-3C_1\frac{\partial^2 W_{xz}}{\partial x\partial y}+\frac{\partial^2 Y_{yz}}{\partial y^2}-3C_1\frac{\partial^2 W_{yz}}{\partial y^2}\right)=0,\\
&\delta\theta_y: \ \frac{\partial M_{xy}}{\partial x}-C_1\frac{\partial P_{xy}}{\partial x}+\frac{\partial M_y}{\partial y}-C_1\frac{\partial P_y}{\partial y}-(Q_y-3C_1R_y)-\frac{1}{2}\left(\frac{\partial X_x}{\partial x}-3C_1\frac{\partial Z_x}{\partial x}+\frac{\partial X_{xy}}{\partial y}-3C_1\frac{\partial Z_{xy}}{\partial y}-\frac{\partial X_z}{\partial x}+3C_1\frac{\partial Z_z}{\partial x}+\frac{\partial^2 Y_{xz}}{\partial x^2}-\right.\\
&\left.3C_1\frac{\partial^2 W_{xz}}{\partial x^2}+\frac{\partial^2 Y_{yz}}{\partial x\partial y}-3C_1\frac{\partial^2 W_{yz}}{\partial x\partial y}\right)=0,
\end{aligned}
\tag{14}
$$

Finally, the governing equations in terms of the FG-CNTRC microplate displacement are obtained and presented in Appendix A by substituting Equation (12) into Equation (14).

The corresponding boundary conditions for clamped and simply supported boundary conditions are as follows:

Clamped (C) edge:

$$
\begin{aligned}
u=v=w=\theta_x=\theta_y=\frac{\partial w}{\partial x}=0 \ &\rightarrow \ x=0,a,\\
u=v=w=\theta_x=\theta_y=\frac{\partial w}{\partial y}=0 \ &\rightarrow \ y=0,b,
\end{aligned}
\tag{15}
$$

Simply supported (S) edge:

$$
\begin{aligned}
v=w=\theta_y=N_x=M_x-C_1P_x+\frac{1}{2}\left(X_{xy}-3C_1Z_{xy}\right)=P_x=0 \ &\rightarrow \ x=0,a,\\
u=w=\theta_x=N_y=M_y-C_1P_y-\frac{1}{2}\left(X_{xy}-3C_1Z_{xy}\right)=P_y=0 \ &\rightarrow \ y=0,b,
\end{aligned}
\tag{16}
$$

## 3. Solution Method

DQM [57,58] is used to discretize the governing Equations (A1)–(A5) and their corresponding boundary conditions (15)–(16) to solve them. By using suitable weighting coefficients, this technique transforms the differential equations into an algebraic equation of the first order. The weighting coefficients are independent of the nature of the problem and only depend on the grid resolution. In other words, at a discontinuous point in a defined domain ($0<x<a$ and $0<y<b$), the partial derivatives of a function (let's call it $w$) are approximated as a set of linear weighting coefficients. However, partial derivatives of the function $f(x_i,y_j)$ at the position $(x_i,y_j)$ are written as in the DQM [58,59]:

$$
\begin{aligned}
&f_x^n(x_i,y_j)=\sum_{K=1}^{N} g_{iK}^{(n)} f(x_K,y_j)\begin{Bmatrix} n=1,2,\ldots,N-1\\ i=1,2,\ldots,N\end{Bmatrix},\\
&f_y^m(x_i,y_j)=\sum_{l=1}^{M} d_{jl}^{(m)} f(x_i,y_j)\begin{Bmatrix} m=1,2,\ldots,M-1\\ j=1,2,\ldots,M\end{Bmatrix},\\
&f_{xy}^{(n+m)}(x_i,y_j)=\sum_{K=1}^{N}\sum_{l=1}^{M} g_{iK}^{(n)} d_{jl}^{(m)} f(x_K,y_l)\begin{Bmatrix} n+m=2,..,N-1\\ i=1,2,\ldots,N\\ j=1,2,\ldots,M\end{Bmatrix}
\end{aligned}
\tag{17}
$$

in which $N$ and $M$ denote the number of grid points in the $x$ and $y$ directions, respectively. The weighting coefficients for the $n$ th-order derivative in the $x$ and $y$ directions are denoted by $g_{ij}^{(n)}$ and $d_{ij}^{(n)}$, respectively, which can be defined as follows:

For the first-order derivative, $n=1$:

$$
g_{iK}^{1}=\frac{M(X_i)}{(X_i-X_K)M(X_K)} i,K=1,2,\ldots,N, \ \ K\neq i
\tag{18}
$$

where

$$M(X_i) = \prod_{\substack{k=1 \\ k \neq i}}^{N} (X_i - X_K) \tag{19}$$

The weighting coefficients for larger derivatives ($n > 1$) can be calculated using the following recursion relationships

$$g_{iK}^{(n)} = n\left(g_{ii}^{(n-1)} g_{iK}^{(1)} - \frac{g_{iK}^{(n-1)}}{X_i - X_K}\right) \begin{Bmatrix} i, K = 1, 2, \ldots, NK \neq i \\ n = 2, 3, \ldots, N-1 \end{Bmatrix} \tag{20}$$

and

$$g_{ii}^{(n)} = -\sum_{K=1}^{N} g_{iK}^{(n)} \begin{Bmatrix} i = 1, 2, \ldots, NK \neq i \\ n = 1, 2, \ldots, N-1 \end{Bmatrix} \tag{21}$$

The DQM can be implemented with any number of discrete grid points and any distribution of grid points. It has been demonstrated, however, that the grid point distribution, which is based on the widely established Gauss–Chebyshev–Lobatto points [58,59], produces findings that are sufficiently precise. The coordinates of the grid points are as follows based on the Gauss–Chebyshev–Lobatto grid point distribution:

$$x_i = \frac{a}{2}\left\{1 - \cos\left[\frac{(i-1)\pi}{(N-1)}\right]\right\}, y_j = \frac{b}{2}\left\{1 - \cos\left[\frac{(j-1)\pi}{(M-1)}\right]\right\} \tag{22}$$

By inserting Equation (17) into the governing Equations (A1)–(A5) and their corresponding boundary conditions (15)–(16) and making various simplifications, the following matrix form is obtained as

$$([K_{tot}] - F^*[I])\{\Gamma\} = 0 \tag{23}$$

in which $I$ signifies the identity matrix and $F^*$ denotes the buckling load. A classic eigenvalue solver can solve Equation (23). The number of discrete mesh points employed in the current DQM (i.e., $N = M$) is the same in both the $x$ and $y$ directions.

## 4. Results and Discussion

### *4.1. Model Validation and Convergence Checking*

The validation and convergence analysis of the created model are covered here. Note that the physical and geometric criteria used in this section and subsequent sections are as follows:

$$E_m = 2.1GPa,\ E_{11}^{CNT} = 5.6466TPa,\ E_{22}^{CNT} = 7.08TPa,\ G_{12}^{CNT} = 1.9445TPa,\ \vartheta_{12}^{CNT} = 0.175,\ \vartheta_m = 0.24 \tag{24}$$

In addition, Table 1 lists the CNT efficiency metrics for different volume fractions [57]. After eliminating the length scale parameter, the current model is used to calculate the non-dimensional buckling load $\overline{N}_{cr} = \frac{F^* a^2}{D_{11}}$ of an FG-CNTRC plate subjected to uniform uniaxial compressive pressure in fully clamped and simply supported boundary conditions, and the results are compared with those from [60] in Table 2. As the DQM procedure's findings are dependent on the number of grid points, a convergence test is also conducted in Table 2. Good agreement can be seen between the predicted buckling values and the data reported in the later reference.

**Table 1.** Efficiency coefficients for different CNT volume fractions.

| $V^*_{CNT}$ | Efficiency Parameters | | |
|---|---|---|---|
| | $\zeta_1$ | $\zeta_2$ | $\zeta_3$ |
| 0.11 | 0.149 | 0.934 | 0.934 |
| 0.14 | 0.15 | 0.941 | 0.941 |
| 0.17 | 0.14 | 1.381 | 1.381 |

**Table 2.** Convergence test and comparison of dimensionless buckling load of an FG-CNTRC plate subjected to uniform uniaxial compressive pressure.

| B.C | Types | Element Mesh | | | | | Ref. [60] |
|---|---|---|---|---|---|---|---|
| | | 5×5 | 7×7 | 9×9 | 11×11 | 13×13 | |
| SSSS | UD | 13.5834 | 14.1105 | 14.1091 | 14.1078 | 14.1078 | 14.1073 |
| | FG-O | 8.2569 | 9.6432 | 9.8357 | 9.8314 | 9.8314 | 9.8306 |
| | FG-X | 15.8670 | 16.8605 | 17.0809 | 17.0642 | 17.0642 | 17.0631 |
| CCCC | UD | 24.2967 | 25.4071 | 25.6825 | 25.7338 | 25.7338 | 25.7329 |
| | FG-O | 19.6568 | 20.7710 | 21.0564 | 21.1230 | 21.1230 | 21.1221 |
| | FG-X | 25.9276 | 27.5414 | 27.8009 | 27.8893 | 27.8893 | 27.8882 |

In another example, Table 3 compares the non-dimensional critical buckling loads $\overline{N}_{cr} = \frac{F^* b^2}{\pi^2 D_{11}}$ of thin, isotropic plates subjected to uniform uniaxial compressive pressure under simply supported boundary conditions found with the current solution to those reported by [61,62] for different aspect ratios. The plate was compressed uniaxially in the x direction. Using the law $h(y) = h_0(1 + \alpha y)$, $\alpha = \frac{h_1 - h_0}{h_0}$, the thickness varies linearly along the $y$ axis. For different aspect ratios, our results show excellent agreement with those reported in the literature. Please refer to the cited references for further information on the effect of the aspect ratio on buckling load performance.

**Table 3.** Comparison of the non-dimensional critical buckling loads of an elastic plate with variable thickness subjected to uniform uniaxial compressive pressure.

| $\frac{a}{b}$ | $\alpha$ | Present | Ref. [61] | Ref. [62] |
|---|---|---|---|---|
| 0.5 | 0.125 | 7.45 | 7.46 | 7.46 |
| | 0.5 | 11.56 | 11.61 | 11.61 |
| 1.5 | 0.125 | 5.19 | 5.19 | 5.19 |
| | 0.5 | 8.22 | 8.23 | 8.23 |

Finally, as seen in Figure 2, using the current approach, the buckling load for various values of the length scale parameter have been computed and compared with the details available in [63] for a square microplate with uniform thickness subjected to uniform uniaxial compressive pressure. For a number of length scale parameters, there is very good agreement between our results and those of [63], which confirms the findings of our approach.

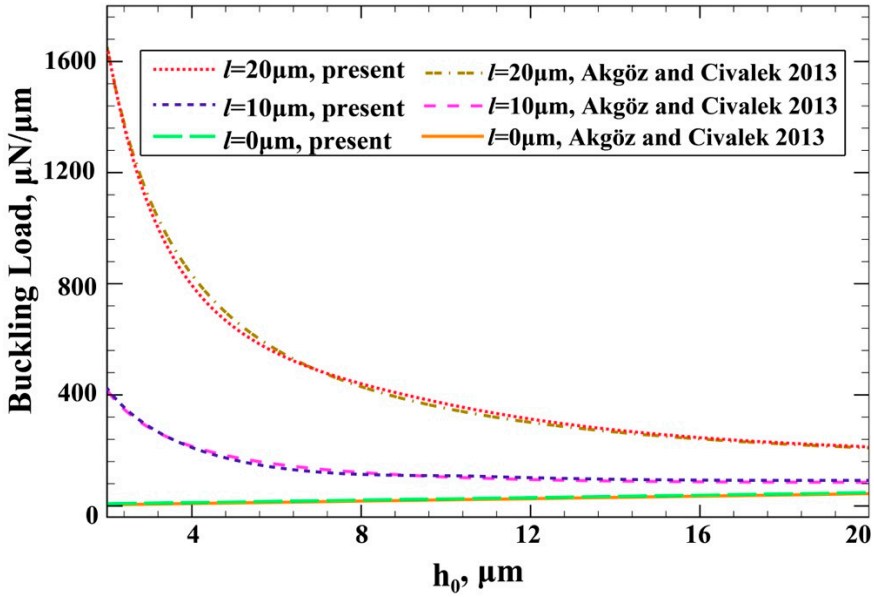


**Figure 2.** Comparison study of the buckling load of a uniform microplate with the details available in Ref. [63] subjected to uniform uniaxial compressive pressure for different values of length scale parameter versus thickness ($a = b = 50h_0$).

### *4.2. Parametric Study*

In this section, numerical examples are presented to examine the influences of the percentage change of thickness, the material length scale parameter to thickness ratio, nonuniform edge loads, boundary conditions, volume percentage of the CNTs, CNT distribution, and elastic medium parameter on the dimensionless buckling load $\overline{N}_{cr} = \frac{F^* a^2}{D_0}$, $D_0 = \frac{E_m {h_0}^3}{12(1-\vartheta_m{}^2)}$ of the FG-CNTRC microplate. The thickness of the microplate is expected to vary in the $y$ direction according to the law $h = h_0\left(1 + \alpha y^{\beta}\right)$, where $\beta$ indicates a non-uniform characteristic for a microplate with variable thickness. Depending on the value of the non-uniform parameter, the y-axis thickness will display a range of patterns. If $\beta = 0$, for instance, the plate's height remains the same in both the x and y axes. If we set $\beta = 1$, we see a linear relationship between thickness ($h_0$) at $y = 0$ and thickness ($h_1$) at $y = b$. At the value of two for the non-uniform parameter ($\beta = 2$), the thickness ($h$) varies parabolically along the y axis.

Figures 3–5 illustrate the variations of the dimensionless biaxial buckling load of the UD-CNTRC microplate against the material length scale parameter to thickness ratio $\left(\frac{l}{h_0}\right)$ for different boundary conditions (SSSS, CCSS, CCCC) and different values of the elastic medium stiffness parameter under uniform (Figure 3), sinusoidal (Figure 4), and reverse sinusoidal (Figure 5) edge compressive loads. It is assumed that $h_0 = \frac{a}{10}$, and a = b, $V^*_{CNT} = 0.11$. The boundary conditions have a significant impact on the variability of the dimensionless biaxial buckling load. Additionally, as anticipated, the buckling load for the CCCC boundary condition has the largest value, which results from the high stiffness effect of this kind of boundary condition on the structure. On the other hand, the structure has the highest buckling load when subjected to reverse sinusoidal load and the lowest buckling load when subjected to sinusoidal load. This may be because, in the case of inverse sinusoidal load, most of the load is distributed towards the edges of the FG-CNTRC microplate, where the microplate's stiffness is substantially greater. As demonstrated by these figures, the critical buckling load increases as the material length scale parameter to thickness ratio increases. Since the couple stress effect adds bending stiffness that grows with $\left(\frac{l}{h_0}\right)$, the total bending stiffness and critical buckling load also grow with $\left(\frac{l}{h_0}\right)$. It can be shown that the dimensionless buckling load decreases with a rise in the non-uniform parameter

($\beta$). This is because the average stiffness of the microplate decreases as the non-uniform parameter increases. The buckling load is found to be proportional to the thickness difference between the microplate's ends and the elastic medium stiffness parameter. As can be observed, the influence of the non-uniform parameter on buckling reduces as the material length scale parameter to thickness ratio rises; however, the influence of the thickness difference increases.

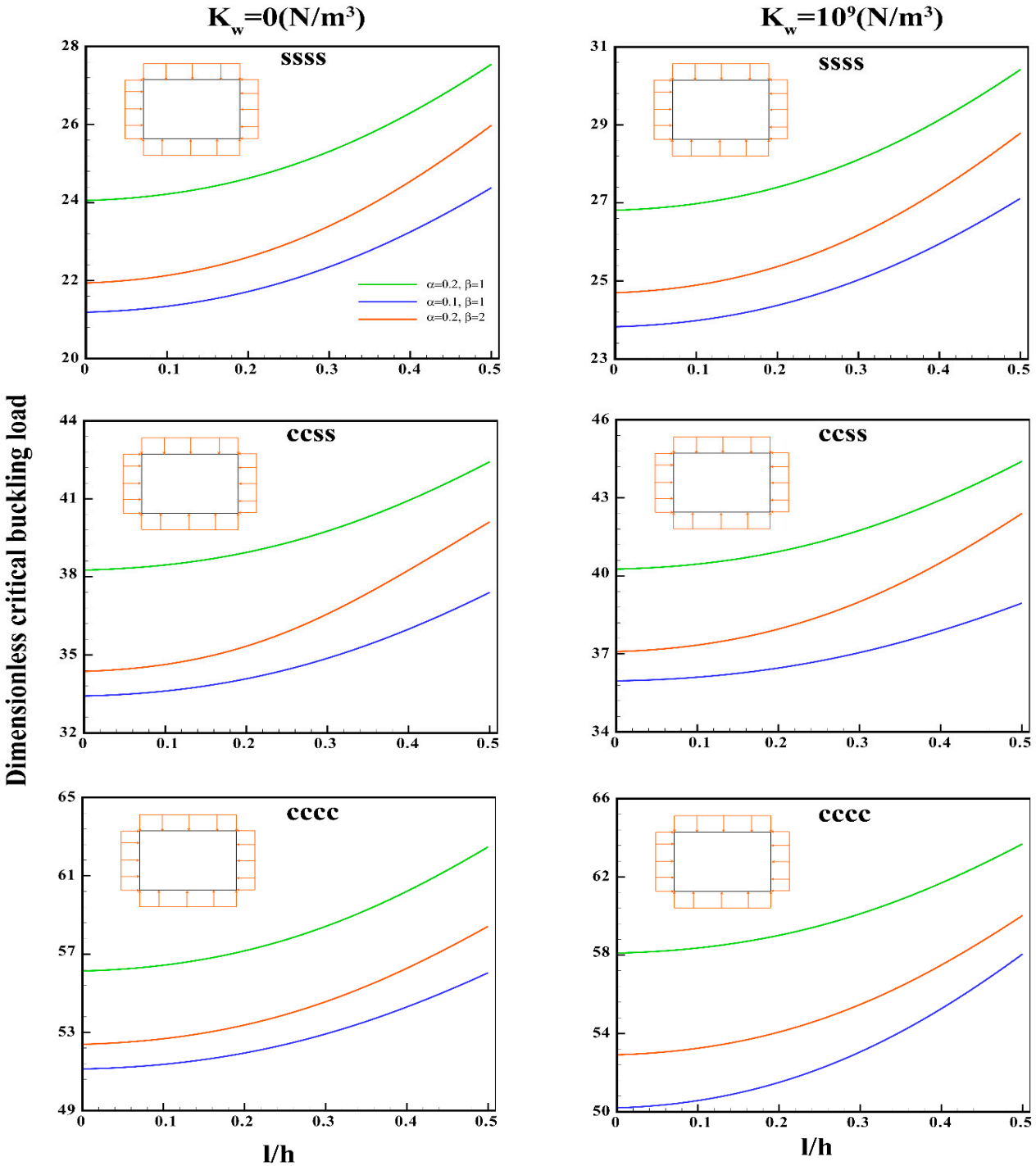


**Figure 3.** Variations of the dimensionless biaxial buckling load of the UD-CNTRC microplate against the material length scale parameter to thickness ratio for different boundary conditions and different values of the elastic medium stiffness parameter (uniform edge compressive load).

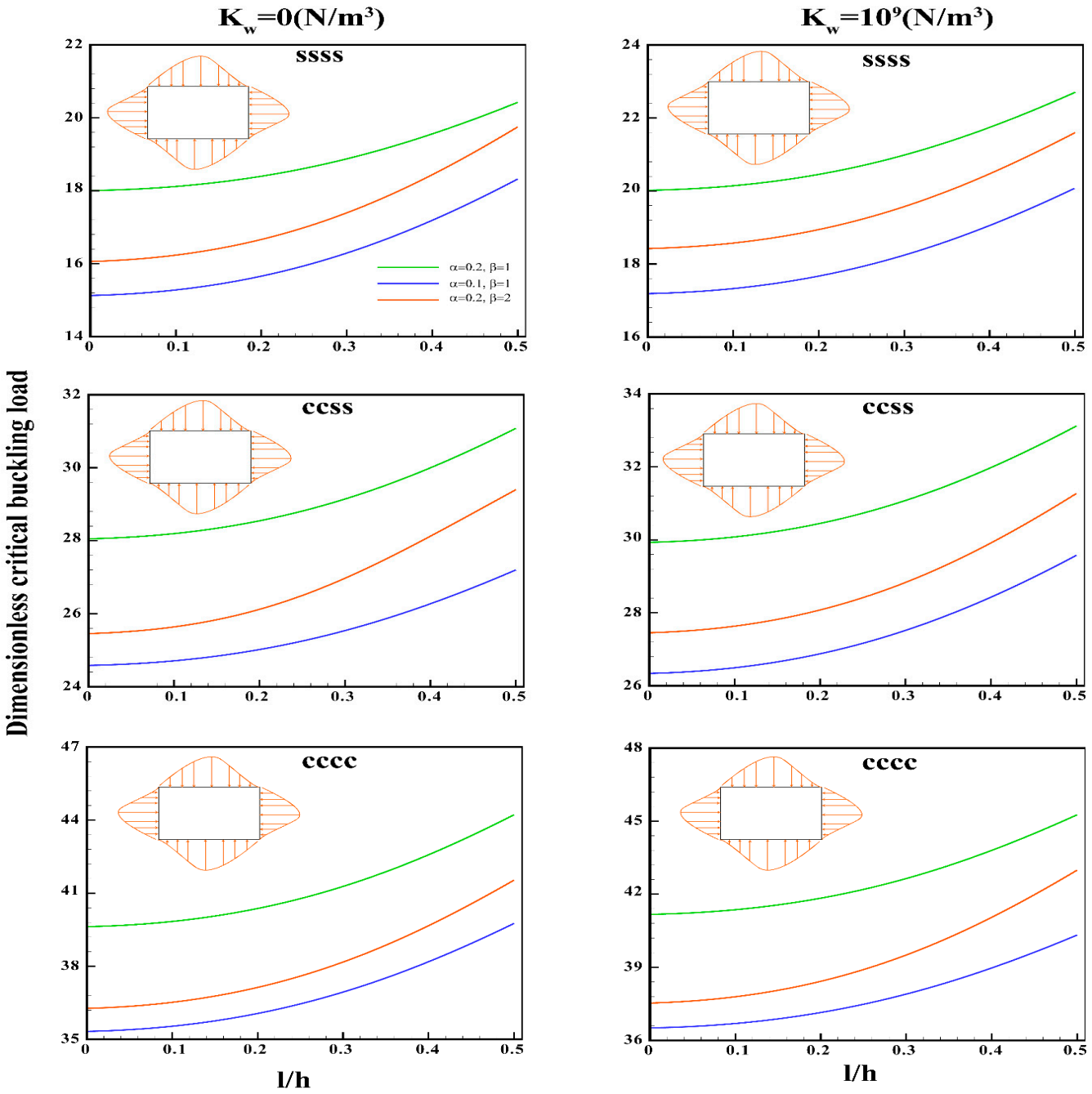


**Figure 4.** Variations of the dimensionless biaxial buckling load of the UD-CNTRC microplate against the material length scale parameter to thickness ratio for different boundary conditions and different values of the elastic medium stiffness parameter (sinusoidal edge compressive load).

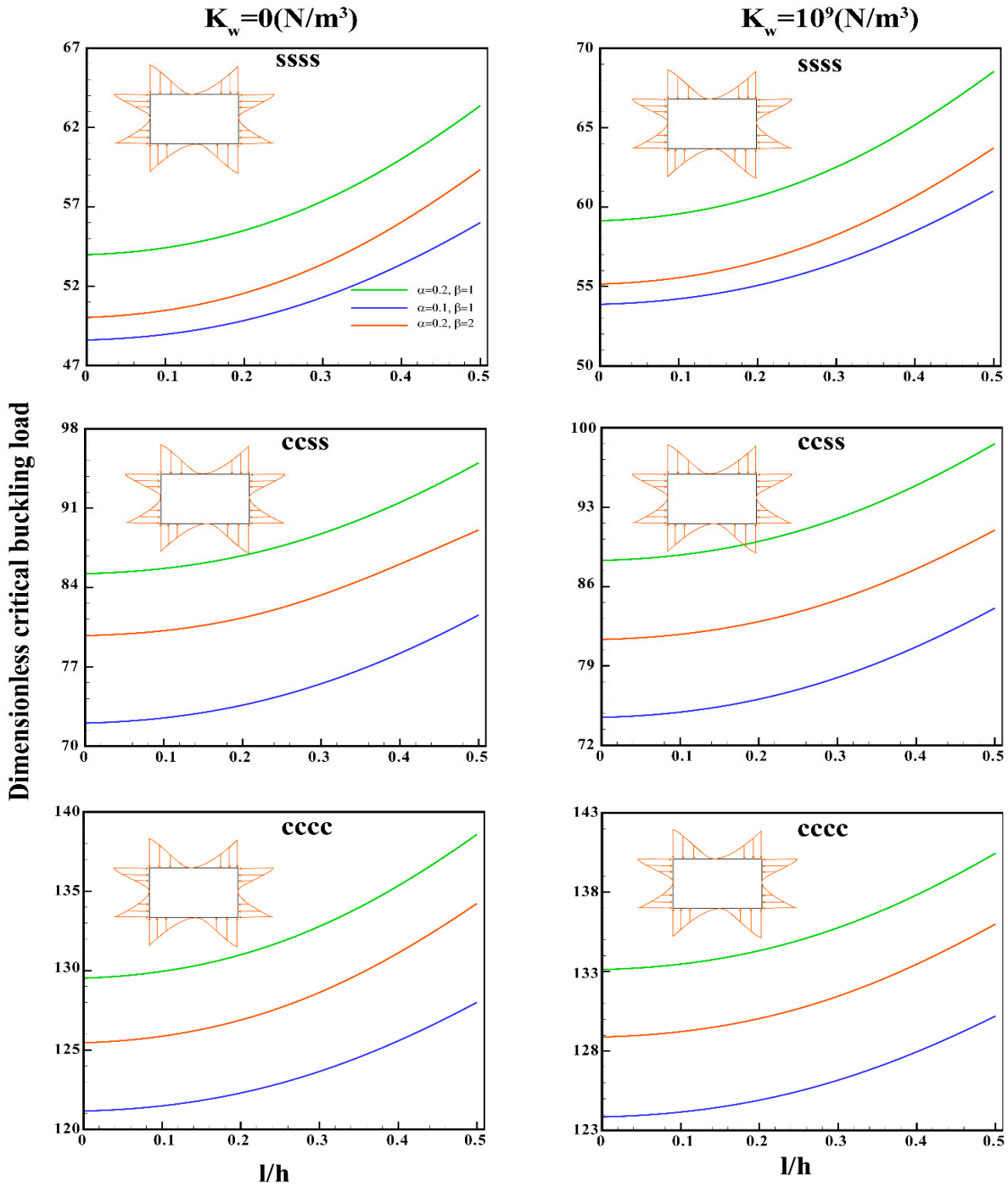


**Figure 5.** Variations of the dimensionless biaxial buckling load of the UD-CNTRC microplate against the material length scale parameter to thickness ratio for different boundary conditions and different values of the elastic medium stiffness parameter (reverse sinusoidal edge compressive load).

Figures 6–8 present the effects of the CNT distributions on the uniaxial and biaxial buckling loads of the FG-CNTRC microplate against the material length scale parameter to thickness ratio $\left(\frac{l}{h_0}\right)$ for different boundary conditions (SSSS, CCSS, CCCC) under uniform (Figure 6), sinusoidal (Figure 7), and reverse sinusoidal (Figure 8) edge compressive loads. It is assumed that $h_0 = \frac{a}{10}, a = b,\ V^*_{CNT} = 0.11,\ k_w = 0,\ \alpha = 0$. These figures show that the critical buckling load for biaxial compression is significantly lower than for uniaxial compression because stiffness is reduced when loads are applied in both the horizontal and vertical planes. Based on these findings, FG-X microplates have higher buckling load values

than UD microplates for all possible CNT distributions, while FG-O microplates have lower values than UD microplates. The physical causes of this behavior are as follows: For the FG-X type, the number of CNTs on the bottom and top of the FG-CNTRC microplate is made as high as possible. This makes the structure of the system more rigid and strong. The results indicate that FG-X > UD > FG-O is the stiffness order for the FG-CNTRC microplates.

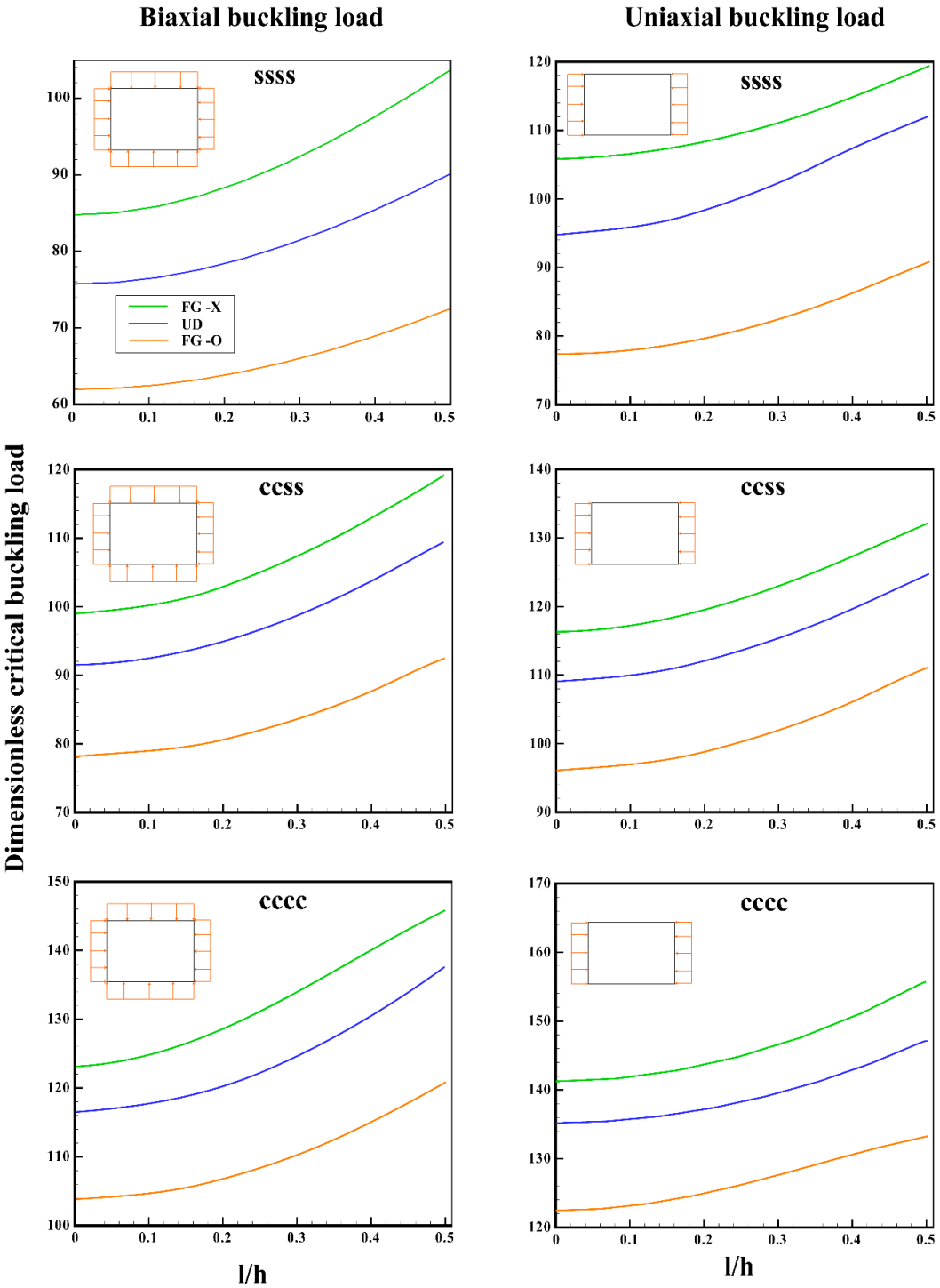


**Figure 6.** The effects of the CNT distributions on the uniaxial and biaxial buckling loads of the FG-CNTRC microplate against the material length scale parameter to thickness ratio (uniform edge compressive load).

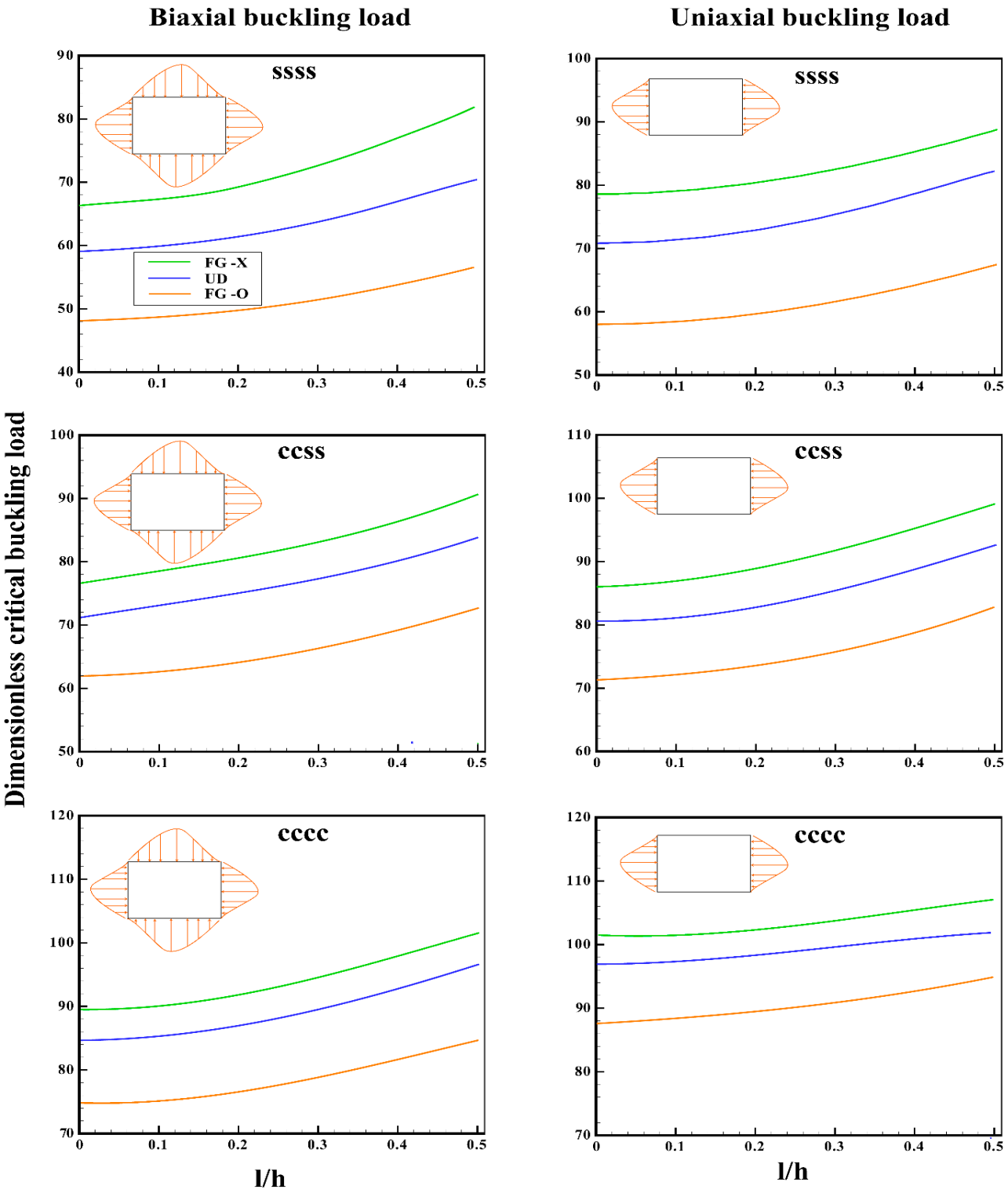


**Figure 7.** The effects of the CNT distributions on the uniaxial and biaxial buckling loads of the FG-CNTRC microplate against the material length scale parameter to thickness ratio (sinusoidal edge compressive load).

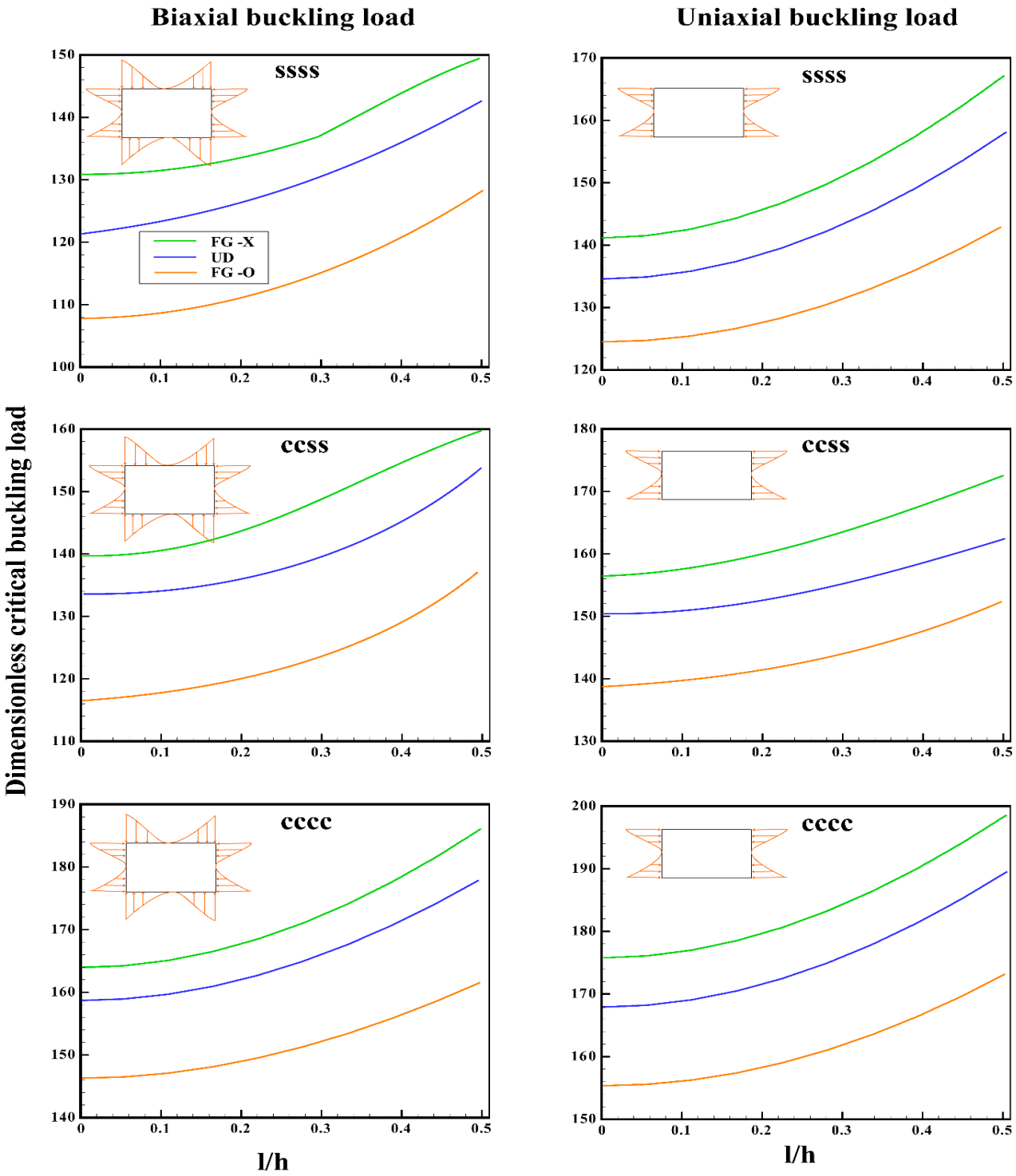


**Figure 8.** The effects of the CNT distributions on the uniaxial and biaxial buckling loads of the FG-CNTRC microplate against the material length scale parameter to thickness ratio (reverse sinusoidal edge compressive load).

Tables 4–6 show the effects of the CNT distributions, CNT volume fractions, and length to thickness ratio on the variations of the dimensionless biaxial buckling load of the FG-CNTRC microplate under uniform and nonuniform edge loads for different boundary conditions when $\frac{l}{h_0} = 0.1, a = b,\ k_w = 0,\ \alpha = 0$. Thus, the buckling load of the FG-CNTRC microplates has a higher value when the volume fraction of CNT is greater. This is because the stiffness of the CNTRC microplates increases when the value of the CNT volume

fraction rises. Furthermore, as shown in these tables, increasing the length to thickness ratio increases the total stiffness of the structure and, as a result, the dimensionless buckling load. Based on the tables, the effects of CNT distributions on buckling changes are amplified when the microplate is subjected to reverse sinusoidal loading.

**Table 4.** The effects of the CNT distributions, CNT volume fractions, and length to thickness ratio on the variations of the dimensionless biaxial buckling load of the FG-CNTRC microplate under uniform and nonuniform edge loads (SSSS).

| Load Cases | $V^*_{CNT}$ | $a/h_0$ | UD | FG-O | FG-X |
|---|---|---|---|---|---|
| Uniform load | 0.11 | 10 | 76.3982 | 62.4456 | 85.6194 |
| | | 20 | 108.6706 | 78.6910 | 134.0614 |
| | 0.14 | 10 | 82.8363 | 67.4566 | 92.5827 |
| | | 20 | 123.6956 | 87.7549 | 147.3007 |
| Sine load | 0.11 | 10 | 59.4015 | 48.5749 | 66.5321 |
| | | 20 | 84.6411 | 61.3355 | 102.4814 |
| | 0.14 | 10 | 64.3922 | 52.4675 | 71.9237 |
| | | 20 | 96.2908 | 68.3911 | 112.2957 |
| Inverse sine load | 0.11 | 10 | 109.2032 | 124.1952 | 132.7104 |
| | | 20 | 192.4701 | 142.7652 | 229.9330 |
| | 0.14 | 10 | 137.7109 | 116.9394 | 146.7540 |
| | | 20 | 227.1229 | 164.4443 | 269.8629 |

**Table 5.** The effects of the CNT distributions, CNT volume fractions, and length to thickness ratio on the variations of the dimensionless biaxial buckling load of the FG-CNTRC microplate under uniform and nonuniform edge loads (CCSS).

| Load Cases | $V^*_{CNT}$ | $a/h_0$ | UD | FG-O | FG-X |
|---|---|---|---|---|---|
| Uniform load | 0.11 | 10 | 92.7860 | 79.2604 | 99.2072 |
| | | 20 | 149.6673 | 116.2542 | 170.1263 |
| | 0.14 | 10 | 98.7655 | 84.5839 | 106.6632 |
| | | 20 | 163.0214 | 128.1712 | 185.1515 |
| Sine load | 0.11 | 10 | 70.7530 | 62.8014 | 76.2244 |
| | | 20 | 113.5681 | 89.0498 | 128.6020 |
| | 0.14 | 10 | 75.2025 | 64.7786 | 81.0391 |
| | | 20 | 123.3760 | 97.9230 | 139.7811 |
| Inverse sine load | 0.11 | 10 | 134.3347 | 118.1731 | 141.0803 |
| | | 20 | 248.9409 | 196.2968 | 281.2835 |
| | 0.14 | 10 | 141.6780 | 126.8329 | 148.2357 |
| | | 20 | 279.8703 | 224.8863 | 310.8059 |

**Table 6.** The effects of the CNT distributions, CNT volume fractions, and length to thickness ratio on the variations of the dimensionless biaxial buckling load of the FG-CNTRC microplate under uniform and nonuniform edge loads (CCCC).

| Load Cases | $V^*_{CNT}$ | $a/h_0$ | UD | FG-O | FG-X |
|---|---|---|---|---|---|
| Uniform load | 0.11 | 10 | 116.5609 | 104.5692 | 124.5312 |
| | | 20 | 200.8065 | 167.8815 | 221.3473 |
| | 0.14 | 10 | 123.0866 | 108.5070 | 130.5892 |
| | | 20 | 215.0219 | 181.3804 | 237.6610 |
| Sine load | 0.11 | 10 | 84.9358 | 75.2791 | 89.8126 |
| | | 20 | 145.5112 | 121.6703 | 160.8139 |
| | 0.14 | 10 | 89.5611 | 79.5182 | 94.8094 |
| | | 20 | 156.0347 | 130.9422 | 172.8222 |
| Inverse sine load | 0.11 | 10 | 160.4343 | 148.0554 | 164.2181 |
| | | 20 | 403.4661 | 370.3635 | 450.0608 |
| | 0.14 | 10 | 194.8202 | 168.3681 | 202.8523 |
| | | 20 | 447.2782 | 391.7958 | 476.9338 |

## 5. Conclusions

This paper reports our examination of the small-scale effect on the stability of a rectangular FG-CNTRC microplate with varying thickness under non-uniform biaxial compression resting on an elastic medium using MCST in combination with TSDT. The extended rule of mixture is used to evaluate the characteristics of the material in the thickness. The DQM was used to solve the derived equations for various combinations of simply supported or clamped boundary conditions. By comparing the established model to data from previous studies, its accuracy and correctness were assessed. A comprehensive numerical analysis was performed to investigate the impact of thickness variations, length scale parameter, nonuniform edge loads, boundary conditions, CNT volume fractions, CNT distributions, and elastic medium parameters on the buckling load. From our findings, we can draw the following conclusions:

The structure has the highest buckling load when it is subjected to reverse sinusoidal load and the lowest buckling load when it is subjected to sinusoidal load. This may be because, in the case of inverse sinusoidal load, most of the load is distributed towards the edges of the FG-CNTRC microplate, where the microplate's stiffness is substantially greater.

The dimensionless buckling load decreases with a rise in the non-uniform parameter ($\beta$). This is because the average stiffness of the microplate decreases as the non-uniform parameter increases.

The buckling load is found to be proportional to the thickness difference between the microplate's ends.

FG-X microplates have higher buckling load values than UD microplates for all possible CNT distributions, while FG-O microplates have lower values than UD microplates.

The effects of CNT distributions on buckling changes are amplified when the microplate is subjected to reverse sinusoidal loading.

**Author Contributions:** Conceptualization, P.R.S., C.T.; validation, P.R.S., C.T.; investigation, W.S.; resources P.R.S., W.S., C.T.; data curation, P.R.S., C.T.; writing— original draft preparation, W.S.; writing—review and editing, W.S.; formal analysis, P.R.S., C.T.; software, P.R.S., C.T.; project administration, P.R.S., W.S.; supervision, P.R.S., W.S., C.T.; All authors have read and agreed to the published version of the manuscript.

**Funding:** This research received no external funding.

**Data Availability Statement:** Data will be made available on request.

**Acknowledgments:** This study was supported by the Thammasat Postdoctoral Fellowship, Thammasat University Research Division, Thammasat University. This Research was also supported by the Thammasat University Research Unit in Structural and Foundation Engineering, Thammasat University. Also, this work was supported by the Thailand Science Research and Innovation Fundamental Fund fiscal year 2023.

**Conflicts of Interest:** The authors declare no conflict of interest.

## Appendix A

$$
\begin{aligned}
\delta u: \quad & A_{11}\frac{\partial^2 u}{\partial x^2} + (B_{11} - C_1 D_{11})\frac{\partial^2 \theta_x}{\partial x^2} - C_1 D_{11}\frac{\partial^3 w}{\partial x^3} + (A_{12} + I_{11})\frac{\partial^2 v}{\partial x \partial y} + (B_{12} - C_1 D_{12} + J_{11} - C_1 L_{11}) \\
& \frac{\partial^2 \theta_y}{\partial x \partial y} + (J_{11} - C_1 L_{11})\frac{\partial^2 \theta_x}{\partial y^2} - (C_1 D_{12} + 2C_1 L_{11})\frac{\partial^3 w}{\partial x \partial y^2} + I_{11}\frac{\partial^2 u}{\partial y^2} + \frac{A_n}{4}\nabla^2\left(\frac{\partial^2 v}{\partial x \partial y} - \frac{\partial^2 u}{\partial y^2}\right) + \\
& \frac{\overline{B}_n}{4}\nabla^2\left(\frac{\partial^2 \theta_y}{\partial x \partial y} - \frac{\partial^2 \theta_x}{\partial y^2}\right) + \frac{3C_1 B_n}{2}\left(\frac{\partial^2 \theta_y}{\partial x \partial y} - \frac{\partial^2 \theta_x}{\partial y^2}\right) + \frac{1}{4}\left\{\frac{\partial B_n}{\partial y} - \frac{\partial C_1}{\partial y}E_n - C_1\frac{\partial E_n}{\partial y}\right\}\left(\frac{\partial^3 \theta_y}{\partial x^3} - \frac{\partial^3 \theta_x}{\partial y \partial x^2}\right) + \\
& \frac{1}{4}\frac{\partial^2 A_n}{\partial y^2}\left(\frac{\partial^2 v}{\partial x \partial y} - \frac{\partial^2 u}{\partial y^2}\right) + \frac{1}{2}\frac{\partial A_n}{\partial y}\left(\frac{\partial^3 v}{\partial x \partial y^2} - \frac{\partial^3 u}{\partial y^3}\right) + \frac{1}{4}\left\{\frac{\partial^2 B_n}{\partial y^2} - \frac{\partial^2 C_1}{\partial y^2}E_n - 2\frac{\partial C_1}{\partial y}\frac{\partial E_n}{\partial y} - C_1\frac{\partial^2 E_n}{\partial y^2}\right\}\left(\frac{\partial^2 \theta_y}{\partial x \partial y} - \frac{\partial^2 \theta_x}{\partial y^2}\right) \\
& + \frac{1}{2}\left\{\frac{\partial B_n}{\partial y} - \frac{\partial C_1}{\partial y}E_n - C_1\frac{\partial E_n}{\partial y}\right\}\left(\frac{\partial^3 \theta_y}{\partial x \partial y^2} - \frac{\partial^3 \theta_x}{\partial y^3}\right) + \frac{\partial I_{11}}{\partial y}\left(\frac{\partial u}{\partial y} + \frac{\partial v}{\partial x}\right) + \frac{\partial J_{11}}{\partial y}\left(\frac{\partial \theta_x}{\partial y} + \frac{\partial \theta_y}{\partial x}\right) + \\
& \frac{1}{4}\frac{\partial A_n}{\partial y}\left(\frac{\partial^3 v}{\partial x^3} - \frac{\partial^3 u}{\partial y \partial x^2}\right) - \left\{3\frac{\partial C_1}{\partial y}\frac{\partial B_n}{\partial y} + \frac{3}{2}\frac{\partial^2 C_1}{\partial y^2}B_n + \frac{3}{2}C_1\frac{\partial^2 B_n}{\partial y^2}\right\}\left(\theta_x + \frac{\partial w}{\partial x}\right) - \left\{\frac{\partial C_1}{\partial y}L_{11} + C_1\frac{\partial L_{11}}{\partial y}\right\} \\
& \left(\frac{\partial \theta_x}{\partial y} + \frac{\partial \theta_y}{\partial x} + 2\frac{\partial^2 w}{\partial x \partial y}\right) + \left\{\frac{3}{2}\frac{\partial C_1}{\partial y}B_n + \frac{3}{2}C_1\frac{\partial B_n}{\partial y}\right\}\left(\frac{\partial \theta_y}{\partial x} + \frac{\partial^2 w}{\partial x \partial y}\right) - 3\left\{\frac{\partial C_1}{\partial y}B_n + C_1\frac{\partial B_n}{\partial y}\right\}\left(\frac{\partial \theta_x}{\partial y} + \frac{\partial^2 w}{\partial x \partial y}\right) = 0
\end{aligned}
\tag{A1}
$$

$$
\begin{aligned}
&\delta v: \ A_{22}\frac{\partial^2 v}{\partial y^2}+(B_{22}-C_1D_{22})\frac{\partial^2\theta_y}{\partial y^2}-C_1D_{22}\frac{\partial^3 w}{\partial y^3}+(A_{12}+I_{11})\frac{\partial^2 u}{\partial x\partial y}+(B_{12}-C_1D_{12}+J_{11}-C_1L_{11})\\
&\frac{\partial^2\theta_x}{\partial x\partial y}+(J_{11}-C_1L_{11})\frac{\partial^2\theta_y}{\partial x^2}-(C_1D_{12}+2C_1L_{11})\frac{\partial^3 w}{\partial x^2\partial y}+I_{11}\frac{\partial^2 v}{\partial x^2}+\frac{A_n}{4}\nabla^2\left(\frac{\partial^2 u}{\partial x\partial y}-\frac{\partial^2 v}{\partial x^2}\right)+\\
&\frac{\overline{B}_n}{4}\nabla^2\left(\frac{\partial^2\theta_x}{\partial x\partial y}-\frac{\partial^2\theta_y}{\partial x^2}\right)+\frac{3C_1B_n}{2}\left(\frac{\partial^2\theta_x}{\partial x\partial y}-\frac{\partial^2\theta_y}{\partial x^2}\right)-\frac{1}{4}\left\{\frac{\partial B_n}{\partial y}-\frac{\partial C_1}{\partial y}E_n-C_1\frac{\partial E_n}{\partial y}\right\}\left(\frac{\partial^3\theta_y}{\partial x^2\partial y}-\frac{\partial^3\theta_x}{\partial x\partial y^2}\right)+\\
&\frac{\partial A_{12}}{\partial y}\frac{\partial u}{\partial x}+\frac{\partial B_{12}}{\partial y}\frac{\partial\theta_x}{\partial x}+\frac{\partial A_{22}}{\partial y}\frac{\partial v}{\partial y}+\frac{\partial B_{22}}{\partial y}\frac{\partial\theta_y}{\partial y}-\frac{1}{4}\frac{\partial A_n}{\partial y}\left(\frac{\partial^3 v}{\partial x^2\partial y}-\frac{\partial^3 u}{\partial x\partial y^2}\right)-\left\{\frac{\partial C_1}{\partial y}D_{22}+C_1\frac{\partial D_{22}}{\partial y}\right\}\\
&\left(\frac{\partial\theta_y}{\partial y}+\frac{\partial^2 w}{\partial y^2}\right)-\left\{\frac{\partial C_1}{\partial y}D_{12}+C_1\frac{\partial D_{12}}{\partial y}-\frac{3}{2}\frac{\partial C_1}{\partial y}B_n-\frac{3}{2}C_1\frac{\partial B_n}{\partial y}\right\}\left(\frac{\partial\theta_x}{\partial x}+\frac{\partial^2 w}{\partial x^2}\right)=0
\end{aligned}
\tag{A2}
$$

$$
\begin{aligned}
&\delta w: \ \left(I_{11}-6C_1M_{11}+9{C_1}^2N_{11}\right)\left(\frac{\partial\theta_x}{\partial x}+\frac{\partial^2 w}{\partial x^2}+\frac{\partial\theta_y}{\partial y}+\frac{\partial^2 w}{\partial y^2}\right)+C_1D_{11}\frac{\partial^3 u}{\partial x^3}+\\
&C_1(H_{11}-C_1K_{11})\frac{\partial^3\theta_x}{\partial x^3}-{C_1}^2K_{11}\frac{\partial^4 w}{\partial x^4}+(C_1D_{12}+2C_1L_{11})\frac{\partial^3 v}{\partial x^2\partial y}+\left(C_1H_{12}-{C_1}^2K_{12}+2C_1N_{11}-2{C_1}^2P_{11}\right)\\
&\frac{\partial^3\theta_y}{\partial x^2\partial y}-\left(2{C_1}^2K_{12}+4{C_1}^2P_{11}\right)\frac{\partial^4 w}{\partial x^2\partial y^2}+(C_1D_{12}+2C_1L_{11})\frac{\partial^3 u}{\partial x\partial y^2}+\left(2C_1N_{11}-2{C_1}^2P_{11}+C_1H_{12}-{C_1}^2K_{12}\right)\\
&\frac{\partial^3\theta_x}{\partial x\partial y^2}+C_1D_{22}\frac{\partial^3 v}{\partial y^3}+C_1(H_{22}-C_1K_{22})\frac{\partial^3\theta_y}{\partial y^3}-C_1K_{22}\frac{\partial^4 w}{\partial y^4}+\frac{\overline{A}_n}{4}\nabla^4 w+9{C_1}^2D_n\left(\frac{\partial\theta_x}{\partial x}+\frac{\partial^2 w}{\partial x^2}+\frac{\partial\theta_y}{\partial y}+\frac{\partial^2 w}{\partial y^2}\right)\\
&+\frac{\check{A}_n}{4}\nabla^2\left(\frac{\partial\theta_x}{\partial x}+\frac{\partial\theta_y}{\partial y}\right)-f_x\left(\frac{\partial^2 w}{\partial x^2}\right)-f_y\left(\frac{\partial^2 w}{\partial y^2}\right)-2f_{xy}\left(\frac{\partial^2 w}{\partial x\partial y}\right)+k_w w+\\
&\left\{\frac{\partial I_{11}}{\partial y}-3\frac{\partial C_1}{\partial y}M_{11}-3C_1\frac{\partial M_{11}}{\partial y}+9C_1\frac{\partial C_1}{\partial y}D_n+9{C_1}^2\frac{\partial D_n}{\partial y}\right\}\left(\theta_y+\frac{\partial w}{\partial y}\right)-\frac{3}{2}C_1\left\{2\frac{\partial D_n}{\partial y}+6\frac{\partial C_1}{\partial y}F_n+6C_1\frac{\partial F_n}{\partial y}\right\}\\
&\frac{\partial^3 w}{\partial x^2\partial y}+\frac{3}{2}C_1\left\{\frac{\partial D_n}{\partial y}-3\frac{\partial C_1}{\partial y}F_n-3C_1\frac{\partial F_n}{\partial y}\right\}\frac{\partial^2\theta_y}{\partial x^2}-\frac{1}{2}\left\{\frac{\partial A_n}{\partial y}+3\frac{\partial C_1}{\partial y}D_n+6C_1\frac{\partial D_n}{\partial y}+9C_1\frac{\partial C_1}{\partial y}F_n+9{C_1}^2\frac{\partial F_n}{\partial y}\right\}\\
&\left(\frac{\partial^3 w}{\partial y^3}-\frac{\partial^3 w}{\partial x^2\partial y}\right)-\frac{1}{4}\left\{\frac{\partial^2 A_n}{\partial y^2}-3\frac{\partial^2 C_1}{\partial y^2}D_n-6\frac{\partial C_1}{\partial y}\frac{\partial D_n}{\partial y}-9C_1\frac{\partial^2 C_1}{\partial y^2}F_n-18C_1\frac{\partial C_1}{\partial y}\frac{\partial F_n}{\partial y}-9{C_1}^2\frac{\partial^2 F_n}{\partial y^2}\right\}\\
&\left(\frac{\partial\theta_x}{\partial x}-\frac{\partial\theta_y}{\partial y}\right)-\frac{1}{2}\left\{\frac{\partial A_n}{\partial y}-3\frac{\partial C_1}{\partial y}D_n-9C_1\frac{\partial C_1}{\partial y}F_n-9{C_1}^2\frac{\partial F_n}{\partial y}\right\}\left(\frac{\partial^2\theta_x}{\partial x\partial y}-\frac{\partial^2\theta_y}{\partial y^2}\right)-\\
&\frac{3}{4}C_1\left\{\frac{\partial^2 D_n}{\partial y^2}+3\frac{\partial^2 C_1}{\partial y^2}F_n+6\frac{\partial C_1}{\partial y}\frac{\partial F_n}{\partial y}+3C_1\frac{\partial^2 F_n}{\partial y^2}\right\}\left(\frac{\partial^2 w}{\partial y^2}-\frac{\partial^2 w}{\partial x^2}\right)-\left\{\frac{\partial A_n}{\partial y}+3\frac{\partial C_1}{\partial y}D_n+3C_1\frac{\partial D_n}{\partial y}\right\}\frac{\partial^3 w}{\partial x^2\partial y}+\\
&\frac{1}{2}\left\{\frac{\partial A_n}{\partial y}-3\frac{\partial C_1}{\partial y}D_n-9C_1\frac{\partial C_1}{\partial y}F_n-9{C_1}^2\frac{\partial F_n}{\partial y}\right\}\frac{\partial^2\theta_x}{\partial x\partial y}+\frac{3}{2}C_1\frac{\partial B_n}{\partial y}\left(\frac{\partial^2 v}{\partial x^2}-\frac{\partial^2 u}{\partial x\partial y}\right)+\frac{3}{2}C_1\left\{\frac{\partial D_n}{\partial y}-\frac{\partial C_1}{\partial y}F_n-C_1\frac{\partial F_n}{\partial y}\right\}\\
&\left(\frac{\partial^2\theta_y}{\partial x^2}-\frac{\partial^2\theta_x}{\partial x\partial y}\right)-\frac{1}{4}\left\{\frac{\partial^2 A_n}{\partial y^2}+3\frac{\partial^2 C_1}{\partial y^2}D_n+6\frac{\partial C_1}{\partial y}\frac{\partial D_n}{\partial y}+3C_1\frac{\partial^2 D_n}{\partial y^2}\right\}\left(\frac{\partial^2 w}{\partial y^2}-\frac{\partial^2 w}{\partial x^2}\right)-C_1\left\{\frac{\partial^2 C_1}{\partial y^2}K_{12}+2\frac{\partial C_1}{\partial y}\frac{\partial K_{12}}{\partial y}+C_1\frac{\partial^2 K_{12}}{\partial y^2}\right\}\\
&\left(\frac{\partial\theta_x}{\partial x}+\frac{\partial^2 w}{\partial x^2}\right)-C_1\left\{\frac{\partial^2 C_1}{\partial y^2}K_{22}+2\frac{\partial C_1}{\partial y}\frac{\partial K_{22}}{\partial y}+C_1\frac{\partial^2 K_{22}}{\partial y^2}\right\}\left(\frac{\partial\theta_y}{\partial y}+\frac{\partial^2 w}{\partial y^2}\right)-2C_1\left\{\frac{\partial C_1}{\partial y}P_{11}+C_1\frac{\partial P_{11}}{\partial y}\right\}\\
&\left(\frac{\partial^2\theta_x}{\partial x\partial y}+\frac{\partial^2\theta_y}{\partial x^2}+2\frac{\partial^3 w}{\partial x^2\partial y}\right)-2C_1\left\{\frac{\partial C_1}{\partial y}K_{12}+C_1\frac{\partial K_{12}}{\partial y}\right\}\left(\frac{\partial^2\theta_x}{\partial x\partial y}+2\frac{\partial^3 w}{\partial x^2\partial y}\right)-2C_1\left\{\frac{\partial C_1}{\partial y}K_{22}+C_1\frac{\partial K_{22}}{\partial y}\right\}\\
&\left(\frac{\partial^2\theta_y}{\partial y^2}+\frac{\partial^3 w}{\partial y^3}\right)+2C_1\frac{\partial N_{11}}{\partial y}\left(\frac{\partial^2\theta_x}{\partial x\partial y}+\frac{\partial^2\theta_y}{\partial x^2}\right)+C_1\frac{\partial^2 D_{12}}{\partial y^2}\frac{\partial u}{\partial x}+2C_1\frac{\partial D_{12}}{\partial y}\frac{\partial^2 u}{\partial x\partial y}+C_1\frac{\partial^2 H_{12}}{\partial y^2}\frac{\partial\theta_x}{\partial x}+\\
&2C_1\frac{\partial H_{12}}{\partial y}\frac{\partial^2\theta_x}{\partial x\partial y}+C_1\frac{\partial^2 D_{22}}{\partial y^2}\frac{\partial v}{\partial y}+2C_1\frac{\partial D_{22}}{\partial y}\frac{\partial^2 v}{\partial y^2}+C_1\frac{\partial^2 H_{22}}{\partial y^2}\frac{\partial\theta_y}{\partial y}+2C_1\frac{\partial H_{22}}{\partial y}\frac{\partial^2\theta_y}{\partial y^2}+2C_1\frac{\partial L_{11}}{\partial y}\left(\frac{\partial^2 u}{\partial x\partial y}+\frac{\partial^2 v}{\partial x^2}\right)+\\
&\frac{1}{2}\left(\frac{\partial A_n}{\partial y}-3\frac{\partial C_1}{\partial y}D_n-3C_1\frac{\partial D_n}{\partial y}\right)\frac{\partial^2\theta_y}{\partial x^2}-3C_1\left\{\frac{\partial M_{11}}{\partial y}-3\frac{\partial C_1}{\partial y}N_{11}-3C_1\frac{\partial N_{11}}{\partial y}\right\}\left(\theta_y+\frac{\partial w}{\partial y}\right)=0
\end{aligned}
\tag{A3}
$$

$$
\begin{aligned}
&\delta\theta_x:\ (B_{11}-C_1D_{11})\tfrac{\partial^2 u}{\partial x^2}+\left(F_{11}-2C_1H_{11}+{C_1}^2K_{11}\right)\tfrac{\partial^2\theta_x}{\partial x^2}-C_1(H_{11}-C_1K_{11})\tfrac{\partial^3 w}{\partial x^3}+\\
&(B_{12}-C_1D_{12}+J_{11}-C_1L_{11})\tfrac{\partial^2 v}{\partial x\partial y}+\left(F_{12}-2C_1H_{12}+{C_1}^2K_{12}+M_{11}-2C_1N_{11}+{C_1}^2P_{11}\right)\\
&\tfrac{\partial^2\theta_y}{\partial x\partial y}-\left(2C_1N_{11}-2{C_1}^2P_{11}+C_1H_{12}-{C_1}^2K_{12}\right)\tfrac{\partial^3 w}{\partial x\partial y^2}+(J_{11}-C_1L_{11})\tfrac{\partial^2 u}{\partial y^2}+\left(M_{11}-2C_1N_{11}+{C_1}^2P_{11}\right)\\
&\tfrac{\partial^2\theta_x}{\partial y^2}-\left(I_{11}-6C_1M_{11}+9{C_1}^2N_{11}\right)\left(\theta_x+\tfrac{\partial w}{\partial x}\right)+\tfrac{\overline{B}_n}{4}\nabla^2\left(\tfrac{\partial^2 v}{\partial x\partial y}-\tfrac{\partial^2 u}{\partial y^2}\right)+\tfrac{3C_1B_n}{2}\left(\tfrac{\partial^2 v}{\partial x\partial y}-\tfrac{\partial^2 u}{\partial y^2}\right)-\\
&\tfrac{\check{A}_n}{4}\nabla^2\tfrac{\partial w}{\partial x}-9{C_1}^2D_n\left(\theta_x+\tfrac{\partial w}{\partial x}\right)+3C_1\overline{D}_n\left(\tfrac{\partial^2\theta_y}{\partial x\partial y}-\tfrac{\partial^2\theta_x}{\partial y^2}\right)+\tfrac{\widetilde{D}_n}{4}\nabla^2\left(\tfrac{\partial^2\theta_y}{\partial x\partial y}-\tfrac{\partial^2\theta_x}{\partial y^2}\right)+\\
&\tfrac{\hat{A}_n}{4}\left(\tfrac{\partial^2\theta_x}{\partial x^2}+4\tfrac{\partial^2\theta_x}{\partial y^2}-3\tfrac{\partial^2\theta_y}{\partial x\partial y}\right)+\tfrac{\partial J_{11}}{\partial y}\left(\tfrac{\partial u}{\partial y}+\tfrac{\partial v}{\partial x}\right)+\tfrac{\partial M_{11}}{\partial y}\left(\tfrac{\partial\theta_x}{\partial y}+\tfrac{\partial\theta_y}{\partial x}\right)+\tfrac{1}{2}\left\{\tfrac{\partial A_n}{\partial y}-3\tfrac{\partial C_1}{\partial y}D_n-3C_1\tfrac{\partial D_n}{\partial y}\right\}\\
&\tfrac{\partial\theta_x}{\partial y}-\tfrac{1}{2}\left\{\tfrac{\partial A_n}{\partial y}-3\tfrac{\partial C_1}{\partial y}D_n-3C_1\tfrac{\partial D_n}{\partial y}\right\}\left(\tfrac{\partial\theta_y}{\partial x}-\tfrac{\partial\theta_x}{\partial y}\right)-3\left\{\tfrac{\partial C_1}{\partial y}\tfrac{\partial D_n}{\partial y}+\tfrac{1}{2}\tfrac{\partial^2 C_1}{\partial y^2}D_n+\tfrac{1}{2}C_1\tfrac{\partial^2 D_n}{\partial y^2}\right\}\left(\theta_x+\tfrac{\partial w}{\partial x}\right)-\\
&\left\{\tfrac{\partial C_1}{\partial y}N_{11}+C_1\tfrac{\partial N_{11}}{\partial y}\right\}\left(\tfrac{\partial\theta_x}{\partial y}+\tfrac{\partial\theta_y}{\partial x}+2\tfrac{\partial^2 w}{\partial x\partial y}\right)+\tfrac{3}{2}\left\{\tfrac{\partial C_1}{\partial y}D_n+C_1\tfrac{\partial D_n}{\partial y}\right\}\left(\tfrac{\partial\theta_y}{\partial x}+\tfrac{\partial^2 w}{\partial x\partial y}\right)-\\
&3\left\{\tfrac{\partial C_1}{\partial y}D_n+C_1\tfrac{\partial D_n}{\partial y}\right\}\left(\tfrac{\partial\theta_x}{\partial y}+\tfrac{\partial^2 w}{\partial x\partial y}\right)-C_1\tfrac{\partial L_{11}}{\partial y}\left(\tfrac{\partial u}{\partial y}+\tfrac{\partial v}{\partial x}\right)-C_1\tfrac{\partial N_{11}}{\partial y}\left(\tfrac{\partial\theta_x}{\partial y}+\tfrac{\partial\theta_y}{\partial x}\right)+C_1\\
&\left\{\tfrac{\partial C_1}{\partial y}P_{11}+C_1\tfrac{\partial P_{11}}{\partial y}\right\}\left(\tfrac{\partial\theta_x}{\partial y}+\tfrac{\partial\theta_y}{\partial x}+2\tfrac{\partial^2 w}{\partial x\partial y}\right)-\tfrac{1}{2}\left\{\tfrac{\partial A_n}{\partial y}+3\tfrac{\partial C_1}{\partial y}D_n+3C_1\tfrac{\partial D_n}{\partial y}\right\}\tfrac{\partial^2 w}{\partial x\partial y}+\\
&\tfrac{3}{4}C_1\left\{\tfrac{\partial D_n}{\partial y}+3\tfrac{\partial C_1}{\partial y}F_n+3C_1\tfrac{\partial F_n}{\partial y}\right\}\tfrac{\partial^2 w}{\partial x\partial y}-\tfrac{3}{2}C_1\left\{\tfrac{\partial D_n}{\partial y}-3\tfrac{\partial C_1}{\partial y}F_n-3C_1\tfrac{\partial F_n}{\partial y}\right\}\tfrac{\partial\theta_x}{\partial y}+\tfrac{3}{2}C_1\left\{\tfrac{\partial D_n}{\partial y}-3\tfrac{\partial C_1}{\partial y}F_n-3C_1\tfrac{\partial F_n}{\partial y}\right\}\\
&\left(\tfrac{\partial\theta_y}{\partial x}-\tfrac{\partial\theta_x}{\partial y}\right)+\tfrac{1}{4}\tfrac{\partial B_n}{\partial y}\left(\tfrac{\partial^3 v}{\partial x^3}-\tfrac{\partial^3 u}{\partial x^2\partial y}\right)+\tfrac{1}{4}\left\{\tfrac{\partial D_n}{\partial y}-\tfrac{\partial C_1}{\partial y}F_n-C_1\tfrac{\partial F_n}{\partial y}\right\}\left(\tfrac{\partial^3\theta_y}{\partial x^3}-\tfrac{\partial^3\theta_x}{\partial x^2\partial y}\right)-\\
&\tfrac{3}{4}C_1\tfrac{\partial E_n}{\partial y}\left(\tfrac{\partial^3 v}{\partial x^3}-\tfrac{\partial^3 u}{\partial x^2\partial y}\right)-\tfrac{3}{4}C_1\left\{\tfrac{\partial F_n}{\partial y}-\tfrac{\partial C_1}{\partial y}H_n-C_1\tfrac{\partial H_n}{\partial y}\right\}\left(\tfrac{\partial^3\theta_y}{\partial x^3}-\tfrac{\partial^3\theta_x}{\partial x^2\partial y}\right)-\tfrac{9}{2}C_1\left\{\tfrac{\partial C_1}{\partial y}F_n+C_1\tfrac{\partial F_n}{\partial y}\right\}\\
&\left(\tfrac{\partial\theta_y}{\partial x}+\tfrac{\partial^2 w}{\partial x\partial y}\right)+\tfrac{1}{4}\tfrac{\partial^2 B_n}{\partial y^2}\left(\tfrac{\partial^2 v}{\partial x\partial y}-\tfrac{\partial^2 u}{\partial y^2}\right)+\tfrac{1}{2}\tfrac{\partial B_n}{\partial y}\left(\tfrac{\partial^3 v}{\partial x\partial y^2}-\tfrac{\partial^3 u}{\partial y^3}\right)+\tfrac{1}{4}\left\{\tfrac{\partial^2 D_n}{\partial y^2}-\tfrac{\partial^2 C_1}{\partial y^2}F_n-2\tfrac{\partial C_1}{\partial y}\tfrac{\partial F_n}{\partial y}-C_1\tfrac{\partial^2 F_n}{\partial y^2}\right\}\\
&\left(\tfrac{\partial^2\theta_y}{\partial x\partial y}-\tfrac{\partial^2\theta_x}{\partial y^2}\right)+\tfrac{1}{2}\left\{\tfrac{\partial D_n}{\partial y}-\tfrac{\partial C_1}{\partial y}F_n-C_1\tfrac{\partial F_n}{\partial y}\right\}\left(\tfrac{\partial^3\theta_y}{\partial x\partial y^2}-\tfrac{\partial^3\theta_x}{\partial y^3}\right)-\tfrac{3}{4}C_1\tfrac{\partial^2 E_n}{\partial y^2}\left(\tfrac{\partial^2 v}{\partial x\partial y}-\tfrac{\partial^2 u}{\partial y^2}\right)-\\
&\tfrac{3}{2}C_1\tfrac{\partial E_n}{\partial y}\left(\tfrac{\partial^3 v}{\partial x\partial y^2}-\tfrac{\partial^3 u}{\partial y^3}\right)-\tfrac{3}{4}C_1\left\{\tfrac{\partial^2 F_n}{\partial y^2}-\tfrac{\partial^2 C_1}{\partial y^2}H_n-2\tfrac{\partial C_1}{\partial y}\tfrac{\partial H_n}{\partial y}-C_1\tfrac{\partial^2 H_n}{\partial y^2}\right\}\left(\tfrac{\partial^2\theta_y}{\partial x\partial y}-\tfrac{\partial^2\theta_x}{\partial y^2}\right)-\\
&\tfrac{3}{2}C_1\left\{\tfrac{\partial F_n}{\partial y}-\tfrac{\partial C_1}{\partial y}H_n-C_1\tfrac{\partial H_n}{\partial y}\right\}\left(\tfrac{\partial^3\theta_y}{\partial x\partial y^2}-\tfrac{\partial^3\theta_x}{\partial y^3}\right)+\tfrac{9}{2}C_1\left\{\tfrac{\partial^2 C_1}{\partial y^2}F_n+2\tfrac{\partial C_1}{\partial y}\tfrac{\partial F_n}{\partial y}+C_1\tfrac{\partial^2 F_n}{\partial y^2}\right\}\left(\theta_x+\tfrac{\partial w}{\partial x}\right)+\\
&9C_1\left\{\tfrac{\partial C_1}{\partial y}F_n+C_1\tfrac{\partial F_n}{\partial y}\right\}\left(\tfrac{\partial\theta_x}{\partial y}+\tfrac{\partial^2 w}{\partial x\partial y}\right)=0
\end{aligned}
\tag{A4}
$$

$$
\begin{aligned}
&\delta\theta_y:\ \ (B_{22}-C_1D_{22})\tfrac{\partial^2 v}{\partial y^2}+\left(F_{22}-2C_1H_{22}+{C_1}^2K_{22}\right)\tfrac{\partial^2\theta_y}{\partial y^2}-C_1(H_{22}-C_1K_{22})\tfrac{\partial^3 w}{\partial y^3}+\\
&(B_{12}-C_1D_{12}+J_{11}-C_1L_{11})\tfrac{\partial^2 u}{\partial x\partial y}+\left(F_{12}-2C_1H_{12}+{C_1}^2K_{12}+M_{11}-2C_1N_{11}+{C_1}^2P_{11}\right)\\
&\tfrac{\partial^2\theta_x}{\partial x\partial y}-\left(2C_1N_{11}-2{C_1}^2P_{11}+C_1H_{12}-{C_1}^2K_{12}\right)\tfrac{\partial^3 w}{\partial x^2\partial y}+(J_{11}-C_1L_{11})\tfrac{\partial^2 v}{\partial x^2}+\left(M_{\,11}-2C_1N_{11}+{C_1}^2P_{11}\right)\\
&\tfrac{\partial^2\theta_y}{\partial x^2}-\left(I_{11}-6C_1M_{11}+9{C_1}^2N_{11}\right)\left(\theta_y+\tfrac{\partial w}{\partial y}\right)+\tfrac{\overline{B}_n}{4}\nabla^2\left(\tfrac{\partial^2 u}{\partial x\partial y}-\tfrac{\partial^2 v}{\partial x^2}\right)+\tfrac{3C_1B_n}{2}\left(\tfrac{\partial^2 u}{\partial x\partial y}-\tfrac{\partial^2 v}{\partial x^2}\right)-\\
&\tfrac{\check{A}_n}{4}\nabla^2\tfrac{\partial w}{\partial y}-9{C_1}^2D_n\left(\theta_y+\tfrac{\partial w}{\partial y}\right)+3C_1\overline{D}_n\left(\tfrac{\partial^2\theta_x}{\partial x\partial y}-\tfrac{\partial^2\theta_y}{\partial x^2}\right)+\tfrac{\widetilde{D}_n}{4}\nabla^2\left(\tfrac{\partial^2\theta_x}{\partial x\partial y}-\tfrac{\partial^2\theta_y}{\partial x^2}\right)+\\
&\tfrac{\hat{A}_n}{4}\left(\tfrac{\partial^2\theta_y}{\partial y^2}+4\tfrac{\partial^2\theta_y}{\partial x^2}-3\tfrac{\partial^2\theta_x}{\partial x\partial y}\right)+\tfrac{\partial B_{12}}{\partial y}\tfrac{\partial u}{\partial x}+\tfrac{\partial F_{12}}{\partial y}\tfrac{\partial\theta_x}{\partial x}+\tfrac{\partial B_{22}}{\partial y}\tfrac{\partial v}{\partial y}+\tfrac{\partial F_{22}}{\partial y}\tfrac{\partial\theta_y}{\partial y}-\tfrac{1}{4}\left\{\tfrac{\partial A_n}{\partial y}-3\tfrac{\partial C_1}{\partial y}D_n-3C_1\tfrac{\partial D_n}{\partial y}\right\}\\
&\left(\tfrac{\partial\theta_x}{\partial x}-\tfrac{\partial\theta_y}{\partial y}\right)-\left\{\tfrac{\partial C_1}{\partial y}H_{12}+C_1\tfrac{\partial H_{12}}{\partial y}\right\}\left(\tfrac{\partial\theta_x}{\partial x}+\tfrac{\partial^2 w}{\partial x^2}\right)-\left\{\tfrac{\partial C_1}{\partial y}H_{22}+C_1\tfrac{\partial H_{22}}{\partial y}+\tfrac{3}{2}\tfrac{\partial C_1}{\partial y}D_n+\tfrac{3}{2}C_1\tfrac{\partial D_n}{\partial y}\right\}\\
&\left(\tfrac{\partial\theta_y}{\partial y}+\tfrac{\partial^2 w}{\partial y^2}\right)+C_1\left\{\tfrac{\partial C_1}{\partial y}K_{12}+C_1\tfrac{\partial K_{12}}{\partial y}\right\}\left(\tfrac{\partial\theta_x}{\partial x}+\tfrac{\partial^2 w}{\partial x^2}\right)-C_1\tfrac{\partial D_{22}}{\partial y}\tfrac{\partial v}{\partial y}-C_1\tfrac{\partial H_{22}}{\partial y}\tfrac{\partial\theta_y}{\partial y}+C_1\\
&\left\{\tfrac{\partial C_1}{\partial y}K_{22}+C_1\tfrac{\partial K_{22}}{\partial y}\right\}\left(\tfrac{\partial\theta_y}{\partial y}+\tfrac{\partial^2 w}{\partial y^2}\right)-\tfrac{1}{4}\left\{\tfrac{\partial A_n}{\partial y}+3\tfrac{\partial C_1}{\partial y}D_n+3C_1\tfrac{\partial D_n}{\partial y}\right\}\left(\tfrac{\partial^2 w}{\partial y^2}-\tfrac{\partial^2 w}{\partial x^2}\right)+\\
&\tfrac{3}{4}C_1\left\{\tfrac{\partial D_n}{\partial y}+3\tfrac{\partial C_1}{\partial y}F_n+3C_1\tfrac{\partial F_n}{\partial y}\right\}\left(\tfrac{\partial^2 w}{\partial y^2}-\tfrac{\partial^2 w}{\partial x^2}\right)+\tfrac{3}{4}C_1\left\{\tfrac{\partial D_n}{\partial y}-3\tfrac{\partial C_1}{\partial y}F_n-3C_1\tfrac{\partial F_n}{\partial y}\right\}\left(\tfrac{\partial\theta_x}{\partial x}-\tfrac{\partial\theta_y}{\partial y}\right)-\\
&\tfrac{1}{4}\tfrac{\partial B_n}{\partial y}\left(\tfrac{\partial^3 v}{\partial x^2\partial y}-\tfrac{\partial^3 u}{\partial x\partial y^2}\right)-\tfrac{1}{4}\left\{\tfrac{\partial D_n}{\partial y}-\tfrac{\partial C_1}{\partial y}F_n-C_1\tfrac{\partial F_n}{\partial y}\right\}\left(\tfrac{\partial^3\theta_y}{\partial x^2\partial y}-\tfrac{\partial^3\theta_x}{\partial x\partial y^2}\right)+\tfrac{3}{4}C_1\tfrac{\partial E_n}{\partial y}\left(\tfrac{\partial^3 v}{\partial x^2\partial y}-\tfrac{\partial^3 u}{\partial x\partial y^2}\right)+\\
&\tfrac{3}{4}C_1\left\{\tfrac{\partial F_n}{\partial y}-\tfrac{\partial C_1}{\partial y}H_n-C_1\tfrac{\partial H_n}{\partial y}\right\}\left(\tfrac{\partial^3\theta_y}{\partial x^2\partial y}-\tfrac{\partial^3\theta_x}{\partial x\partial y^2}\right)-\tfrac{9}{2}C_1\left\{\tfrac{\partial C_1}{\partial y}F_n+C_1\tfrac{\partial F_n}{\partial y}\right\}\left(\tfrac{\partial\theta_x}{\partial x}+\tfrac{\partial^2 w}{\partial x^2}\right)=0
\end{aligned}
\tag{A5}
$$

where

$$\{A_{11}, B_{11}, F_{11}, D_{11}, H_{11}, K_{11}\} = \int_{-\frac{h(y)}{2}}^{\frac{h(y)}{2}} \frac{E_{11}}{1-\vartheta_{12}\vartheta_{21}}\left\{1, z, z^2, z^3, z^4, z^6\right\}dz,$$

$$\{A_{12}, B_{12}, F_{12}, D_{12}, H_{12}, K_{12}\} = \int_{-\frac{h(y)}{2}}^{\frac{h(y)}{2}} \frac{\vartheta_{12}E_{22}}{1-\vartheta_{12}\vartheta_{21}}\left\{1, z, z^2, z^3, z^4, z^6\right\}dz,$$

$$\{A_{22}, B_{22}, F_{22}, D_{22}, H_{22}, K_{22}\} = \int_{-\frac{h(y)}{2}}^{\frac{h(y)}{2}} \frac{E_{22}}{1-\vartheta_{12}\vartheta_{21}}\left\{1, z, z^2, z^3, z^4, z^6\right\}dz,$$

$$\{A_n, B_n, D_n, E_n, F_n, H_n\} = \int_{-\frac{h(y)}{2}}^{\frac{h(y)}{2}} l^2 G_{12}\left\{1, z, z^2, z^3, z^4, z^6\right\}dz,$$

$$\overline{B}_n = B_n - C_1 E_n,\ \ \overline{D}_n = D_n - C_1 F_n,\ \ \widetilde{D}_n = D_n - 2C_1 F_n + {C_1}^2 H_n,$$

$$\hat{A}_n = A_n - 6C_1 D_n + 9{C_1}^2 F_n, \overline{A}_n = A_n + 6C_1 D_n + 9{C_1}^2 F_n,$$

$$\widetilde{A}_n = A_n - 9{C_1}^2 F_n.$$

## References


1. Ruocco, E.; Reddy, J.N. Buckling analysis of elastic–plastic nanoplates resting on a Winkler–Pasternak foundation based on nonlocal third-order plate theory. *Int. J. Non. Linear. Mech.* **2020**, *121*, 103453. [CrossRef]
2. Jamalpoor, A.; Hosseini, M. Biaxial buckling analysis of double-orthotropic microplate-systems including in-plane magnetic field based on strain gradient theory. *Compos. Part B Eng.* **2015**, *75*, 53–64. [CrossRef]
3. Thai, H.-T.; Vo, T.P. A new sinusoidal shear deformation theory for bending, buckling, and vibration of functionally graded plates. *Appl. Math. Model.* **2013**, *37*, 3269–3281. [CrossRef]
4. Liew, K.M.; Peng, L.X.; Kitipornchai, S. Buckling analysis of corrugated plates using a mesh-free Galerkin method based on the first-order shear deformation theory. *Comput. Mech.* **2006**, *38*, 61–75. [CrossRef]
5. Bodaghi, M.; Saidi, A.R. Levy-type solution for buckling analysis of thick functionally graded rectangular plates based on the higher-order shear deformation plate theory. *Appl. Math. Model.* **2010**, *34*, 3659–3673. [CrossRef]
6. Ruocco, E.; Zhang, H.; Wang, C.M. Hencky bar-net model for buckling and vibration analyses of rectangular plates with non-uniform thickness. *Eng. Struct.* **2018**, *168*, 653–668.
7. Hamedani, S.J.; Ranji, A.R. Buckling analysis of stiffened plates subjected to non-uniform biaxial compressive loads using conventional and super finite elements. *Thin-Walled Struct.* **2013**, *64*, 41–49. [CrossRef]
8. Ruocco, E.; Reddy, J.N. A discrete differential geometry-based approach to buckling and vibration analyses of inhomogeneous Reddy plates. *Appl. Math. Model.* **2021**, *100*, 342–364. [CrossRef]
9. Rahmouni, F.; Elajrami, M.; Madani, K.; Campilho, R.D. Isogeometric analysis based on non-uniform rational B-splines technology of stress and failure strength in inter-ply hybrid laminated composite. *J. Compos. Mater.* **2022**, *56*, 00219983221105313. [CrossRef]
10. Osiander, R.; Darrin, M.A.G.; Champion, J.L. *MEMS and Microstructures in Aerospace Applications*; CRC Press: Boca Raton, FL, USA, 2018.
11. Syms, R.R.A.; Yeatman, E.M.; Bright, V.M.; Whitesides, G.M. Surface tension-powered self-assembly of microstructures-the state-of-the-art. *J. Microelectromech. Syst.* **2003**, *12*, 387–417.
12. Mindlin, R.D.; Tiersten, H.F. Effects of couple-stresses in linear elasticity. *Arch. Ration Mech. Anal.* **1962**, *11*, 415–448. [CrossRef]
13. Eringen, A.C. Nonlocal polar elastic continua. *Int. J. Eng. Sci.* **1972**, *10*, 1–16. [CrossRef]
14. Sirimontree, S.; Thongchom, C.; Saffari, P.R.; Refahati, N.; Saffari, P.R.; Jearsiripongkul, T.; Keawsawasvong, S. Effects of thermal environment and external mean flow on sound transmission loss of sandwich functionally graded magneto-electro-elastic cylindrical nanoshell. *Eur. J. Mech.* **2023**, *97*, 104774. [CrossRef]
15. Mindlin, R.D.; Eshel, N.N. On first strain-gradient theories in linear elasticity. *Int. J. Solids Struct.* **1968**, *4*, 109–124. [CrossRef]
16. Mindlin, R.D. Second gradient of strain and surface-tension in linear elasticity. *Int. J. Solids Struct.* **1965**, *1*, 417–438. [CrossRef]
17. Lam, D.C.C.; Yang, F.; Chong, A.C.M.; Wang, J.; Tong, P. Experiments and theory in strain gradient elasticity. *J. Mech. Phys. Solids* **2003**, *51*, 1477–1508. [CrossRef]
18. Lim, C.W.; Zhang, G.; Reddy, J.N. A higher-order nonlocal elasticity and strain gradient theory and its applications in wave propagation. *J. Mech. Phys. Solids* **2015**, *78*, 298–313. [CrossRef]
19. Roodgar Saffari, P.; Fakhraie, M.; Roudbari, M.A. Size-Dependent Vibration Problem of Two Vertically-Aligned Single-Walled Boron Nitride Nanotubes Conveying Fluid in Thermal Environment via Nonlocal Strain Gradient Shell Model. *J. Solid Mech.* **2021**, *13*, 164–185.

20. Roodgar Saffari, P.; Fakhraie, M.; Roudbari, M.A. Free vibration problem of fluid-conveying double-walled boron nitride nanotubes via nonlocal strain gradient theory in thermal environment. *Mech. Based Des. Struct. Mach.* **2020**, *50*, 3665–3682. [CrossRef]
21. Saffari, P.R.; Fakhraie, M.; Roudbari, M.A. Nonlinear vibration of fluid conveying cantilever nanotube resting on visco-pasternak foundation using non-local strain gradient theory. *Micro Nano Lett.* **2020**, *15*, 181–186. [CrossRef]
22. Zarabimanesh, Y.; Roodgar Saffari, P.; Roudgar Saffari, P.; Refahati, N. Hygro-thermo-mechanical vibration of two vertically aligned single-walled boron nitride nanotubes conveying fluid. *J. Vib. Control* **2022**, *28*, 2101–2120. [CrossRef]
23. Thongchom, C.; Roodgar Saffari, P.; Roudgar Saffari, P.; Refahati, N.; Sirimontree, S.; Keawsawasvong, S.; Titotto, S. Dynamic response of fluid-conveying hybrid smart carbon nanotubes considering slip boundary conditions under a moving nanoparticle. *Mech. Adv. Mater Struct.* **2022**, 1–14. [CrossRef]
24. Yang, F.; Chong, A.C.M.; Lam, D.C.C.; Tong, P. Couple stress based strain gradient theory for elasticity. *Int. J. Solids Struct.* **2002**, *39*, 2731–2743. [CrossRef]
25. Ma, H.M.; Gao, X.-L.; Reddy, J.N. A microstructure-dependent Timoshenko beam model based on a modified couple stress theory. *J. Mech. Phys. Solids* **2008**, *56*, 3379–3391. [CrossRef]
26. Kahrobaiyan, M.H.; Asghari, M.; Ahmadian, M.T. A Timoshenko beam element based on the modified couple stress theory. *Int. J. Mech. Sci.* **2014**, *79*, 75–83. [CrossRef]
27. Tsiatas, G.C. A new Kirchhoff plate model based on a modified couple stress theory. *Int. J. Solids Struct.* **2009**, *46*, 2757–2764. [CrossRef]
28. Shaat, M.; Mahmoud, F.F.; Gao, X.-L.; Faheem, A.F. Size-dependent bending analysis of Kirchhoff nano-plates based on a modified couple-stress theory including surface effects. *Int. J. Mech. Sci.* **2014**, *79*, 31–37. [CrossRef]
29. Shang, Y.; Mao, Y.-H.; Cen, S.; Li, C.-F. Generalized conforming Trefftz element for size-dependent analysis of thin microplates based on the modified couple stress theory. *Eng. Anal. Bound. Elem.* **2021**, *125*, 46–58. [CrossRef]
30. Wu, C.-P.; Hsu, C.-H. A three-dimensional weak formulation for stress, deformation, and free vibration analyses of functionally graded microscale plates based on the consistent couple stress theory. *Compos. Struct.* **2022**, *296*, 115829. [CrossRef]
31. Refahati, N.; Jearsiripongkul, T.; Thongchom, C.; Saffari, P.R.; Saffari, P.R.; Keawsawasvong, S. Sound transmission loss of double-walled sandwich cross-ply layered magneto-electro-elastic plates under thermal environment. *Sci. Rep.* **2022**, *12*, 16621. [CrossRef]
32. Vo, D.; Suttakul, P.; Rungamornrat, J.; Nanakorn, P. Static analysis of planar arbitrarily curved microbeams with the modified couple stress theory and Euler-Bernoulli beam model. *Appl. Math. Model.* **2022**, *112*, 358–390. [CrossRef]
33. Qi, Z.; Peng, W.; He, T. Investigation on the thermoelastic response of a nanobeam in modified couple stress theory considering size-dependent and memory-dependent effects. *J. Therm. Stress* **2022**, *45*, 773–792. [CrossRef]
34. Al-Furjan, M.S.H.; Samimi-Sohrforozani, E.; Habibi, M.; won Jung, D.; Safarpour, H. Vibrational characteristics of a higher-order laminated composite viscoelastic annular microplate via modified couple stress theory. *Compos. Struct.* **2021**, *257*, 113152. [CrossRef]
35. Yu, X.; Fan, X.; Bi, X. Size-dependent frequency analysis of the magneto-electro-elastic rotary microdisk by incorporating modified couple stress and higher-order shear deformation theories. *Mech. Based Des. Struct. Mach.* **2021**, 1–20. [CrossRef]
36. Thanh, C.-L.; Tran, L.V.; Vu-Huu, T.; Abdel-Wahab, M. The size-dependent thermal bending and buckling analyses of composite laminate microplate based on new modified couple stress theory and isogeometric analysis. *Comput. Methods Appl. Mech. Eng.* **2019**, *350*, 337–361. [CrossRef]
37. Lou, J.; He, L.; Yang, J.; Kitipornchai, S.; Wu, H. Size and foundation effects on the vibration of buckled functionally graded microplates within the modified couple stress theory framework. *Int. J. Appl. Mech.* **2018**, *10*, 1850068. [CrossRef]
38. Zhang, C.; Eyvazian, A.; Alkhedher, M.; Alwetaishi, M.; Ahammad, N.A. Modified couple stress theory application to analyze mechanical buckling behavior of three-layer rectangular microplates with honeycomb core and piezoelectric face sheets. *Compos. Struct.* **2022**, *292*, 115582. [CrossRef]
39. Afshari, H.; Adab, N. Size-dependent buckling and vibration analyses of GNP reinforced microplates based on the quasi-3D sinusoidal shear deformation theory. *Mech. Based Des. Struct. Mach.* **2022**, *50*, 184–205. [CrossRef]
40. Dresselhaus, M.S.; Dresselhaus, G.; Eklund, P.C.; Rao, A.M. Carbon nanotubes. In *The Physics of Fullerene-Based and Fullerene-Related Materials. Physics and Chemistry of Materials with Low-Dimensional Structures*; Springer: New York, NY, USA, 2000; pp. 331–379.
41. Dai, H. Carbon nanotubes: Opportunities and challenges. *Surf. Sci.* **2002**, *500*, 218–241. [CrossRef]
42. Iijima, S.; Ichihashi, T. Single-shell carbon nanotubes of 1-nm diameter. *Nature* **1993**, *363*, 603. [CrossRef]
43. Tan, H.; Jiang, L.Y.; Huang, Y.; Liu, B.; Hwang, K.C. The effect of van der Waals-based interface cohesive law on carbon nanotube-reinforced composite materials. *Compos. Sci. Technol.* **2007**, *67*, 2941–2946. [CrossRef]
44. Ci, L.; Suhr, J.; Pushparaj, V.; Zhang, X.; Ajayan, P.M. Continuous carbon nanotube reinforced composites. *Nano Lett.* **2008**, *8*, 2762–2766. [CrossRef] [PubMed]
45. Thongchom, C.; Jearsiripongkul, T.; Refahati, N.; Roudgar Saffari, P.; Roodgar Saffari, P.; Sirimontree, S.; Keawsawasvong, S. Sound transmission loss of a honeycomb sandwich cylindrical shell with functionally graded porous layers. *Buildings* **2022**, *12*, 151. [CrossRef]

46. Thongchom, C.; Saffari, P.R.; Refahati, N.; Saffari, P.R.; Pourbashash, H.; Sirimontree, S.; Keawsawasvong, S. An analytical study of sound transmission loss of functionally graded sandwich cylindrical nanoshell integrated with piezoelectric layers. *Sci. Rep.* **2022**, *12*, 3048. [CrossRef]
47. Vaishali, T.; Mukhopadhyay, T.; Naskar, S.; Dey, S. On machine learning assisted data-driven bridging of FSDT and HOZT for high-fidelity uncertainty quantification of laminated composite and sandwich plates. *Compos. Struct.* **2022**, *304*, 116276. [CrossRef]
48. Li, X.; Wang, H.; Li, G. Reanalysis assisted metaheuristic optimization for free vibration problems of composite laminates. *Compos. Struct.* **2018**, *206*, 380–391. [CrossRef]
49. Savran, M.; Aydin, L. Stochastic optimization of graphite-flax/epoxy hybrid laminated composite for maximum fundamental frequency and minimum cost. *Eng. Struct.* **2018**, *174*, 675–687. [CrossRef]
50. Shen, H.-S. Nonlinear bending of functionally graded carbon nanotube-reinforced composite plates in thermal environments. *Compos. Struct.* **2009**, *91*, 9–19. [CrossRef]
51. Zhang, G.; Xiao, C.; Rahimi, A.; Safarpour, M. Thermal and mechanical buckling and vibration analysis of FG-GPLRC annular plate using higher order shear deformation theory and generalized differential quadrature method. *Int. J. Appl. Mech.* **2020**, *12*, 2050019. [CrossRef]
52. Thai, C.H.; Ferreira, A.J.M.; Rabczuk, T.; Nguyen-Xuan, H. Size-dependent analysis of FG-CNTRC microplates based on modified strain gradient elasticity theory. *Eur. J. Mech.* **2018**, *72*, 521–538. [CrossRef]
53. Cheshmeh, E.; Karbon, M.; Eyvazian, A.; Jung D won Habibi, M.; Safarpour, M. Buckling and vibration analysis of FG-CNTRC plate subjected to thermo-mechanical load based on higher order shear deformation theory. *Mech. Based Des. Struct. Mach.* **2022**, *50*, 1137–1160. [CrossRef]
54. Phung-Van, P.; Thai, C.H. A novel size-dependent nonlocal strain gradient isogeometric model for functionally graded carbon nanotube-reinforced composite nanoplates. *Eng. Comput.* **2022**, *38*, 2027–2040. [CrossRef]
55. Reddy, J.N. A simple higher-order theory for laminated composite plates. *J. Appl. Mech. Dec.* **1984**, *51*, 745–752. [CrossRef]
56. Roodgar Saffari, P.; Fakhraie, M.; Roudbari, M.A. Free Vibration and Transient Response of Heterogeneous Piezoelectric Sandwich Annular Plate Using Third-Order Shear Deformation Assumption. *J. Solid Mech.* **2020**, *12*, 315–333. [CrossRef]
57. Phung-Van, P.; Abdel-Wahab, M.; Liew, K.M.; Bordas, S.P.A.; Nguyen-Xuan, H. Isogeometric analysis of functionally graded carbon nanotube-reinforced composite plates using higher-order shear deformation theory. *Compos. Struct.* **2015**, *123*, 137–149. [CrossRef]
58. Shu, C. *Differential Quadrature and Its Application in Engineering*; Springer Science & Business Media: London, UK, 2012.
59. Bert, C.W.; Malik, M. Differential quadrature method in computational mechanics: A review. *Appl. Mech. Rev.* **1996**, *49*, 1–28. [CrossRef]
60. Lei, Z.X.; Liew, K.M.; Yu, J.L. Buckling analysis of functionally graded carbon nanotube-reinforced composite plates using the element-free kp-Ritz method. *Compos. Struct.* **2013**, *98*, 160–168. [CrossRef]
61. Farajpour, A.; Danesh, M.; Mohammadi, M. Buckling analysis of variable thickness nanoplates using nonlocal continuum mechanics. *Phys. E Low-Dimens. Syst. Nanostruct.* **2011**, *44*, 719–727. [CrossRef]
62. Eisenberger, M.; Alexandrov, A. Buckling loads of variable thickness thin isotropic plates. *Thin-Walled Struct.* **2003**, *41*, 871–889. [CrossRef]
63. Akgöz, B.; Civalek, Ö. Modeling and analysis of micro-sized plates resting on elastic medium using the modified couple stress theory. *Meccanica* **2013**, *48*, 863–873. [CrossRef]